JAERI - M
90-088

MTX MICROWAVE-ELECTRIC-FIELD DIAGNOSTIC

June 1990

Kazuo ODAJIMA, Kazumi OHASA, Makoto SHIHO, Toshiatsu ODA[*1]
Ken TAKIYAMA[*1], Katsu MIZUNO[*2], James H. FOOTE[*3]
David G. NILSON[*3], Steven L. ALLEN[*3] and Thomas A. CASPER[*3]

日 本 原 子 力 研 究 所
Japan Atomic Energy Research Institute

JAERI-Mレポートは，日本原子力研究所が不定期に公刊している研究報告書です。
入手の問合わせは，日本原子力研究所技術情報部情報資料課（〒319-11茨城県那珂郡東海村）あて，お申しこしください。なお，このほかに財団法人原子力弘済会資料センター（〒319-11 茨城県那珂郡東海村日本原子力研究所内）で複写による実費頒布をおこなっております。

JAERI-M reports are issued irregularly.
Inquiries about availability of the reports should be addressed to Information Division, Department of Technical Information, Japan Atomic Energy Research Institute, Tokai-mura, Naka-gun, Ibaraki-ken 319-11, Japan.

編集兼発行　日本原子力研究所
印　　刷　㈱原子力資料サービス

JAERI-M 90-088

MTX Microwave-Electric-Field Diagnostic

Kazuo ODAJIMA, Kazumi OHASA, Makoto SHIHO, Toshiatsu ODA[*1]
Ken TAKIYAMA[*1], Katsu MIZUNO[*2], James H. FOOTE[*3]
David G. NILSON[*3], Steven L. ALLEN[*3] and Thomas A. CASPER[*3]

Department of Thermonuclear Fusion Research
Naka Fusion Research Establishment
Japan Atomic Energy Research Institute
Naka-machi, Naka-gun, Ibaraki-ken

(Received May 17, 1990)

A joint Japan-U.S. project is in progress to measure the high electric fields produced by a free-electron laser beam of GW-peak-power level when injected into the plasma of the Microwave Tokamak Experiment (MTX) at the Lawrence Livermore National Laboratory in California. In this report, we discuss the planned method of measurement and the status of the work. The equipment needed is either well along in the design stage or is being built. We plan to test out the combined operation of all components in Japan before shipping to Livermore. Although the measurement appears difficult for a variety of technical and physics reasons, calculations indicate that it should be possible.

Keywords: Laser-Aided Particle-Probe Spectroscopy, Electric-Field Diagnostic, MTX, Microwave Tokamak Experiment, FEL, Free-Electron Laser, ECRH, Electron Cyclotron Resonance Heating

---

*1 Hiroshima University
*2 Plasma Physics Research Institute (University of California)
*3 Lawrence Livermore National Laboratory (LLNL)

JAERI－M 90－088

ＭＴＸ用マイクロ波電界測定器

日本原子力研究所那珂研究所核融合研究部
小田島 和男 ・ 大麻 和美 ・ 志甫 諒 ・ 尾田 年充 [*1]
多幾山 憲[*1]・ Katsu MIZUNO [*2]・ James H. FOOTE [*3]
David G.NILSON [*3]・Steven L.ALLEN [*3]・Thomas A.CASPER [*3]

（1990年5月17日受理）

米国・ローレンスリバモア国立研究所（ＬＬＮＬ）において進められている自由電子レーザー（ＦＥＬ）のマイクロ波を用いてプラズマを加熱する実験計画・ＭＴＸ計画においてプラズマ中のギガワットレベルのピーク電力を持つＦＥＬマイクロ波の電界を測定する計画が日米の協力で進められている。現在測定原理に基づき設計，一部においては製作が進められている。本報告書においてその測定原理と作業の現状について報告する。

この測定器のすべてのコンポーネントを1990年中にそろえて，1991年1月から原研において総合調整を行った後リバモアに送り出す予定である。本測定は物理的にも，技術的にも高いレベルが要求されるが，充分な理論的検討によって測定の目途がたった。

那珂研究所：〒311－01 茨城県那珂郡那珂町大字向山801－1
*1 広島大学
*2 プラズマ物理研究所（カリフォルニア大学）
*3 ローレンスリバモア国立研究所

Contents

目　　次

1. INTRODUCTION

Foote

In the Microwave Tokamak Experiment (MTX) [1] at the Lawrence Livermore National Laboratory (LLNL), ultra-high-power microwaves are injected into the toroidal plasma region for plasma heating and current drive. Peak power levels up to 150 MW already have been attained with a free-electron laser (FEL) beam, and preparations are being made to inject FEL power in the range of 1-2 GW. One of the key goals for MTX is to understand the propagation and absorption mechanisms of the microwaves in the tokamak plasma. This understanding is essential in guiding the use of microwaves with ultra-high peak power for plasma heating, noninductive current drive, and other plasma processes.

We are preparing a spectroscopic method for measuring the spatially varying FEL microwave electric field in the MTX plasma. This approach combines laser-induced-fluorescence spectroscopy with a neutral-particle beam (Laser-Aided Particle Probe Spectroscopy, or LAPPS). Thus, we need a neutral-particle beam with sufficient particle current, a high-power tunable dye laser, and an efficient light-collecting and detecting system to measure the low level of resulting light.

This crossed-beam measurement requires the spatial and temporal intersection of the FEL electron-heating beam, the neutral-helium beam, and the laser beam, not an easy task in the crowded region where the FEL beam enters the MTX plasma. In addition, this intersection must be viewed by collimated optics. Figure 1 shows schematically the interaction region for the LAPPS diagnostic and the principal components of the system. An overall view of the MTX experimental area and the location of the LAPPS equipment is shown in Fig. 2.

Similar measurements, but under less severe plasma conditions, have been made in the past. Using the Stark effect, spectroscopic measurements of electron-cyclotron-frequency electric fields have been satisfactorily made in model-type plasmas by combining a neutral-beam probe and laser-induced fluorescence [2,3]. The same technique has been modified to also measure relatively low-frequency fields such as at the ion-cyclotron frequency in a plasma device [4]. This low-frequency measurement determined the plugging electric field in the line cusp of the RFC-XX-M experiment at Nagoya University. The

experimental result compares well with theory and provides confidence that the technique can be applied to large plasma experiments. However, MTX has much higher densities and temperatures than available in the earlier experiments, so that the details of the measurement will be different and, in general, the measurement will be more difficult.

One of the most difficult problems, because of attenuation, is to provide a sufficient density of radiating atoms at the center of the burned-out and highly collisional plasma without significantly perturbing the plasmas. Helium is an attractive candidate because of its low ionization cross section. We estimate that a sufficient density of radiating helium atoms can be obtained at the center of the MTX plasma with a helium neutral-beam probe.

We plan to use metastable helium atoms because then dye-laser energies are available to pump these atoms to higher excited states. Metastable atoms in the triplet state can be produced in a xenon-gas helium-neutralizing chamber, while those in the singlet state can be produced by collisional excitation in the MTX plasma itself.

There are several possible spectroscopic schemes that we may be able to use, each one with its advantages and disadvantages. We are designing the equipment to allow as wide range of choice as feasible.

The microwave electric field in a FEL beam in the MTX plasma is expected to be as large as several hundred kV/cm. Calculations show that, because of the Stark effect, forbidden transitions can be strongly excited in such a high electric field. By measuring the intensity of emitted light resulting from a forbidden transition, we will be able to estimate the microwave electric field. This emitted-light intensity varies approximately as the square of the electric field.

To measure the light emitted from the states excited by the laser beam, we need a collimated optical system with wavelength filtering to view the interaction region and to transport the light away from the plasma region to conveniently located detectors. Because of the limited access to the MTX plasma region, our field of view is restricted. Photon counting rates are expected to be low, so extra effort is needed to minimize background and noise levels.

Besides measuring the FEL electric field, it also may be possible using this method to measure the lower electric field of a gyrotron-produced electron-heating beam injected into the MTX plasma. Although

the pulses are of lower power, they are of longer duration.

The equipment we are developing may have other diagnostic applications, too. Examples are measurements of ion temperature using charge-exchange recombination (CXR), fully stripped impurity densities, edge-impurity states, and possibly the radial profile of the magnetic field.

Personnel from both Japan and the United States are working on this project. Those with responsibilities and their affiliations are listed in Table 1. Three group discussion and planning meetings have already taken place, the first at LLNL during October 26-30, 1989, the second at the Tokai site of the Japan Atomic Energy Research Institute (JAERI) during January 30 to February 2, 1990, and the third at LLNL during April 2-6, 1990. Much progress in the planning was made at these three meetings and in the periods between them.

Although decisions concerning details of this diagnostic system will continue to be made as our work progresses, the project is presently advanced enough so that preparing this Status Report seemed advisable. In this way, interested persons not directly involved in this work will have a summary of our planning. The Table of Contents lists the sections of this report and their principal authors. We have indicated in the report where information is still being gathered and where decisions still need to be made.

We have also prepared a paper for the "Eighth Topical Conference on High Temperature Plasma Diagnostics", held at Hyannis, Massachusetts during May 6-10, 1990. The proceedings of this conference will be published in the journal Review of Scientific Instruments later this year. The abstract for our conference paper is reproduced in the Appendix of this report. References [5-7] are other publications concerning this work.

2. PRINCIPLE OF MEASUREMENT

Oda, Mizuno

In this section, we discuss the principle and basic physics of the LAPPS measurement technique and we outline the application to MTX in a general way. Details will be given in Sec. 3 and in subsequent sections of this report.

2.1 Stark Effect

It is well recognized that the forbidden lines or plasma satellite lines due to the Stark effect can be used to directly measure the electric field in plasmas [3, 8-11]. This is the effect that we apply in the LAPPS diagnostic system.

Figure 3(a) shows an energy diagram of the four-level system developed for measurement of static or quasistatic electric fields. Let us assume that the level ℓ is originally well populated; that is, ℓ denotes the ground state or a metastable state. Level i is excited from level ℓ by laser irradiation, where level i is at a higher principal quantum number n than is ℓ. When an electric field is applied, level mixing occurs between the levels i and j. This permits light to be emitted with wavelength corresponding to the forbidden transition from i to k. In this report, we refer to this series of events as an "allowed-excitation" scheme.

To obtain the electric-field strength, only the intensity ratio R of the forbidden line ($i \to k$) to the allowed line ($i \to \ell$) needs to be measured. We have already calculated R for several line pairs of HeI and LiI [12]. For not-too-strong electric fields, R is expressed by

$$R \propto E^2/(\Delta W)^2 \ , \tag{1}$$

where E is the electric-field strength (rms) and ΔW is the energy difference between the levels i and j.

Figure 3(b) shows another energy diagram, this time for a "forbidden-excitation" scheme in which a $\Delta L = 2$ transition occurs upon the absorption of laser light in an electric field (i.e., an $\ell \to j$ transition; L is the angular-momentum quantum number). This process is then followed by emission from level j to level k. The intensity of this emission can also be expressed as a function of electric-field

strength, just as in the allowed-excitation scheme. To determine the field strength in this case, however, we need to perform a calibration measurement involving the level ℓ to level i transition (the laser is retuned to this transition energy). To do this, the spectral intensity distribution of the laser must be known but not the population density of the level ℓ or the absolute intensity of the induced emission.

When a high-frequency electric field is observed, the forbidden line generally has a complicated structure. The ratio R used in Eq. (1) can still be obtained by using the total intensity of the forbidden line, however, provided that the quasi-static approximation is still valid. This is true in the case where the energy difference ΔW is much larger than that corresponding to the electric-field frequency.

Figure 3(c) shows a partial energy-level diagram for HeI, depicting levels pertinent to the LAPPS measurements. In the singlet system, the metastable state 2^1S is used as the lower level ℓ. In the triplet system, the level 2^3P is used for ℓ because 2^3P and the metastable level 2^3S are closely coupled due to electron impact in the dense plasma. To inject the emitting atoms into the plasma, a high-speed atomic-helium beam is used.

2.2 Outline of the Experiment

Tables 2 and 3 show six possible schemes that might be used on MTX for measuring electric fields with LAPPS. These six measurement methods are shown schematically in Fig. 4. The four allowed-excitation schemes in Table 2 correspond to the type discussed in regard to Fig. 3(a), while the two in Table 3, which are forbidden-excitation schemes, correspond to Fig. 3(b).

In Table 2, besides the possible line pairs of HeI that might be used in an allowed-excitation measurement, we also show the calculated values of the line-intensity ratio R for an electric field of 100 kV/cm. (The line intensity is defined as the total number of emitted photons.) In Cases (1) and (2), for example, the 3^1P (or 4^1P) level is resonantly excited from the 2^1S level by a tuned dye laser. When an electric field is applied in the plasma, the forbidden transition 3^1P (or 4^1P) → 2^1P emits photons in addition to the allowed transition 3^1P (or 4^1P) → 2^1S. The ratio R can then be experimentally determined by measuring the intensity of these spectral lines.

Figure 5 shows the configuration for the LAPPS measurements, depicting the relationship between the direction of the FEL electric field, the direction of the MTX magnetic field, the helium and laser beams, and the direction of observation. There are many considerations in planning the apparatus for the LAPPS measurements.

First of all, a helium beam of sufficiently high current must be injected into the center of the MTX plasma. The singlet metastable level 2^1S is strongly produced from the ground state of the helium beam by electron impact in the plasma. On the other hand, the triplet metastable level 2^3S is not greatly produced in the plasma. Thus, we plan to produce this state in the neutralizer that converts the helium ions to neutrals, using xenon gas, for example. The 2^3P level is then excited from the 2^3S level by the plasma by collisions in the plasma.

One of the critical issues for the LAPPS diagnostic is the obtaining of high enough density of metastable atoms to make the electric-field measurements possible. Estimates of densities in the plasma of various helium-atom levels will be described in Sec. 3, using a collisional-radiative model. The total photon numbers emitted from the interaction region of the helium beam, dye-laser beam, and FEL microwave beam will also be estimated.

The optical equipment to collect the emitted light is also an important item. The observation solid angle for the optics should be as large as possible because the number of photons collected by a detector is proportional to the solid angle. Interference filters of narrow wavelength band will be used to select the spectral lines we wish to detect and to filter out unwanted impurity lines. When choosing the filters and the exact laser frequency, we must take into account the Doppler shifts arising from the velocity of the helium-beam atoms.

We need to take the motional Stark effect into consideration because the fast neutral-helium beam traverses magnetic-field lines (see Fig. 5). The electric-field strength E_M in kV/cm that is produced due to this effect is given by

$$E_M = (v_b \times B)/10^7 , \tag{2}$$

where v_b is the beam velocity in cm/s and B is in T. For a helium-beam energy of 50 keV and B = 5 T, the maximum value of E_M is estimated to be 77 kV/cm. This is comparable to the FEL electric-field strength.

Because the applied magnetic field in the present experiment is large, the Zeeman effect should also be considered. Figure 6 shows an example of the Zeeman effect combined with the motional Stark effect and high-frequency effects, for the singlet energy-level system. The resulting line spectrum is schematically shown in Fig. 7.

3. EXCITATION AND IONIZATION OF A FAST NEUTRAL-HELIUM BEAM IN A PLASMA WITH LASER EXCITATION -- COLLISIONAL-RADIATIVE MODEL

Oda, Takiyama

In this section we present equations for calculating the population densities vs position and time of various energy levels of a neutral-helium beam passing through a plasma. We also list values of parameters for the MTX plasma, the FEL beam to be injected into MTX, and the helium beam planned for LAPPS. We then apply these equations and parameter values to the six electric-field-measurement schemes given in Tables 2 and 3, schemes that might be used on MTX. Finally, we present for these six schemes calculated results of possible signal levels that might be detected by the LAPPS system for an FEL electric field of 100 kV/cm. The method of calculation is explained.

3.1 Model

The temporal and spatial evolution of the population density $n_k(x,t)$ of an energy level k in a fast neutral-helium beam being locally irradiated with a pulsed laser beam while passing through a plasma can be written as a set of coupled rate equations:

$$\frac{\partial n_k}{\partial t} + v_b \frac{\partial n_k}{\partial x} = -n_k\Big(\sum_{i<k} A_{ki} + \sum_i n_e(x)\langle\sigma_e v\rangle_{ki} + \sum_i n_p(x)\langle\sigma_p v\rangle_{ki} + n_q(x)\sigma_q v_b \Big)$$

$$+ \Big(\sum_{i>k} n_i A_{ik} + \sum_i n_i n_e(x)\langle\sigma_e v\rangle_{ik} + \sum_i n_i n_p(x)\langle\sigma_p v\rangle_{ik} \Big)$$

$$+ (\delta_{k\ell} - \delta_{km})\, I_{\ell m}(t)(n_m B_{m\ell} - n_i B_{\ell m}), \quad k = 1, \ldots\ldots, 9, \qquad (3)$$

where v_b is the beam velocity, x is the distance traveled in the plasma (the plasma edge is at x = 0 and 30 cm, with the plasma center at x = 15 cm), n_e and n_p are the electron and proton densities, A_{ki} is the radiative transition probability from level k to level i, $\langle\sigma_e v\rangle_{ki}$ and $\langle\sigma_p v\rangle_{ki}$ are summations of excitation and ionization rate coefficients for electron and proton impact, respectively (the proton impact term also includes the charge-exchange processes), and $\sigma_q v_b$ is the rate coefficient for the charge exchange on helium of multiply-charged impurity ions (X^{q+}) whose density is n_q. The last term on the right-

hand side of Eqs. (3) arises for ℓ and m levels because of the dye-laser-beam injection. In that term, $\delta_{k\ell}$ and δ_{km} are Kronecker deltas, $I_{\ell m}(t)$ is the laser power density, and $B_{\ell m} = (g_\ell/g_m)B_{m\ell}$ are Einstein's B coefficients.

When the transition $\ell \to m$ is a forbidden one such as the $\ell \to j$ transition shown in Fig. 3(b), the Einstein B coefficient can be calculated as now described. The perturbed state $|j(F)>$ due to the applied electric field F can be expressed as a linear combination of the unperturbed states $|i>$ with the same principal quantum number:

$$j(F)> = \sum_i C_{ji}|i> \ .$$

Here, C_{ji} is calculated by a quantum-mechanical procedure and the square of its absolute value is the probability of the perturbed state $|j(F)>$ existing in the unperturbed state $|i>$. Then, the B coefficient is given by

$$B_{i\ell} = |C_{ji}|^2 \cdot B_{i\ell} \ ,$$

were B_{il} is the value for the allowed transition $i \to \ell$, and it can be obtained from the corresponding Einstein A coefficient.

For our calculations with the model described here, we make several simplifying assumptions. First of all, all ionized atoms are assumed to leave the beam because of the trapping by the magnetic field. Secondly, the incident beam flux is assumed to be constant, so that the spatial distribution of the population densities (with no laser beam) can be obtained by putting $\partial n_k/\partial t = 0$ and $I_{\ell m}(t) = 0$. We also neglect transitions with a spin change between states higher than $n = 2$ (n is the principal quantum number), and we assume that the levels of different angular-momentum quantum number for $n = 4$ and $n = 5$ are at the same energy. Finally, we apply Eqs. (3) using only the following singlet and triplet nine states:

A. singlet $\quad 1^1S,\ 2^1S,\ 2^1P,\ 3^1S,\ 3^1P,\ 3^1D,\ n=4,\ n=5,\ He^+,$

B. triplet $\quad 1^1S,\ 2^3S,\ 2^3P,\ 3^3S,\ 3^3P,\ 3^3D,\ n=4,\ n=5,\ He^+.$

The following parameter values for the plasma, the microwave free-electron laser, and the neutral beam are used in the calculations:

Plasma parameter
- Electron (proton) density 10^{14} cm^{-3}
- Electron (proton) temperature 1 keV
- Plasma diameter 30 cm
- Major impurity ion is C^{6+} and its density is ≈ 1 % of n_e.

FEL
- Peak power several GW
- Frequency 140 GHz
- FEL pulse width 50 ns

Neutral beam
- Beam energy 50 keV (velocity 1.55×10^{8} cm/s)
- Beam current 200 mA
- Beam cross section 2×2 cm^2
- He atomic density
  - A. singlet system --- $n(1^1S) = 2.57 \times 10^9$ cm^{-3}
  - B. triplet system --- $n(1^1S) = 2.06 \times 10^9$ cm^{-3}, $n(2^3S) = 5.1 \times 10^8$ cm^{-3}

Cross-section values for excitation, de-excitation, and ionization by electron impact are available for all levels considered here [13]. However, those for the other atomic processes are considered only for the ground state (1^1S) as follows:

$\sigma_p^{ex}(1^1S\rightarrow2^1S) = 4\times10^{-18}$ cm^2 for proton impact excitation [14],
$\sigma_p^{ion} = 3.2\times10^{-17}$ cm^2 for proton impact ionization [15],
$\sigma_p^{cx} = 1.3\times10^{-16}$ cm^2 for charge exchange of proton on $He(1^1S)$ [15],
$\sigma_x = 1\times10^{-15}$ cm^2 for charge exchange of C^{6+} ion on $He(1^1S)$ [16].

3.2 Results

We now present calculated results for the six cases shown in Tables 2 and 3 and in Fig. 4. These results are given in Figs. 8 − 14 and in Table 4.

Figure 8 shows the calculated spatial distribution, as a function of position in the plasma, of the population densities for the following HeI energy states: (a) 1^1S, 2^1S, 2^1P, 3^1P, 3^1D, $n=4$, and $n=5$ for the singlet; and (b) 2^3S, 2^3P, 3^3P, 3^3D, $n=4$, and $n=5$ for the triplet. These results were calculated using Eqs. (3) with $\partial n_k/\partial t = 0$ and no laser beam present. As shown in Fig. 8(a), about 50 % of the 1^1S ground state still survives at the plasma center ($x=15$ cm). On the other hand, the metastable state 2^3P has been reduced at the plasma center to 1/25 of its initial density, as shown in Fig. 8(b).

The time history of helium-beam components passing through the plasma region is obtained by solving the rate equations [Eqs. (3)] with $\partial n_k/\partial x = 0$. Also, we now assume that the laser beam is turned on, so that the last term on the right side of Eqs. (3) is used. Figure 9(a) shows calculated 2^1S and 3^1P population densities [Case (1) of Table 2] with laser excitation during the transit time of about 30 ns across the plasma central region from x = 12.5 to 17.5 cm (velocity = 1.55×10^8 cm/s).

The calculated rate of photon emission vs time from a unit volume within the observation region (5 cm length assumed) along the helium-beam path through the plasma is plotted in the upper part of Fig. 9(b). In the lower part of this figure, the laser power profile used in the calculations is shown. For values of laser-beam power, spectral width, and duration, we assume 5 kW/cm^2, 0.4 Å, and 50 ns, respectively. The constant-intensity component in the upper part of Fig. 9(b) between 25 and 50 ns (and between 100 and 125 ns) corresponds to the light from particle impact excitation (i.e., "plasma-induced emission light", or PIEL) of the beam. The enhancement between 50 and 100 ns is produced by the laser resonance-absorption excitation (i.e., "laser-induced fluorescence", or LIF). The total photon number N_p emitted per unit volume in the observing time Δt, which corresponds to the assumed laser pulse width of 50 ns, is given by an integration from 50 to 100 ns (see Appendix 2).

Figure 9(c) shows the N_p laser-power dependencies for LIF and for the summation of LIF and PIEL. These are calculated from results such as those in Fig. 9(b).

Similar results for Cases (2) - (6) of Tables 2 and 3 are displayed in Figs. 10 - 14, respectively. Each figure has three parts [(a), (b), and (c)] just as in Fig. 9.

To estimate the number of photoelectrons S_{el} ejected from the photocathode of a photomultiplier (PM) tube, the detector planned for LAPPS, the sensitivity S_{obs} of the whole detection system used for the measurement must be determined. We define the sensitivity as

$$S_{obs} = T_{opt}\, Q_{PM}\, \Delta\Omega/4\pi \ , \tag{4}$$

where T_{opt} is the transmissivity of the optical system, Q_{PM} is the quantum efficiency of the PM tube, and $\Delta\Omega$ is the observation solid

angle. Then S_{el} can be expressed as

$$S_{el} = N_p S_{obs} \cdot \tag{5}$$

Values of N_p are obtained from Figs. 9(c), 10(c), 11(c), 12(c), 13(c), and 14(c).

Numerical results for the six cases of Tables 2 and 3, for applied electric field of 100 kV/cm, are summarized in Table 4. There we assume $T_{opt} = 0.3$, $Q_{PM} = 0.1$, and $\Delta\Omega/4\pi = 1.4 \times 10^{-3}$, so that $S_{obs} = 4.2 \times 10^{-5}$. The injected laser power is given in Table 4 as $I_L(kW/cm^2)$, with wavelength width of 0.04 nm (0.4 Å). The observing time Δt is 50 ns, which also corresponds to the FEL pulse width assumed in the calculation. For the cases where there is a forbidden line (F) as well as an allowed line (A), the calculated value of S_{el} must be allocated between F and A according to the ratio R in Table 2.

Bremsstrahlung contributes to the background light in all six cases. It is estimated for a wavelength of 500 nm, assuming $Z_{eff} = 1.7$. In Cases (5) and (6), PIEL as well as bremsstrahlung should be considered to contribute to the background light because collisions that populate the 3^1D or 3^3D states by passing through other levels also contribute to the light emitted from these two states.

For the forbidden-excitation schemes [Cases (5) and (6)], the calculated signals in Table 4 are relatively large. Our recent computer simulations indicate that we can still obtain adequate signals if we focus the laser to a 1.5 cm height and arrange the optical system to image an area of even smaller height. By focusing onto a small area (and by also operating the laser at a lower intensity than the level at which the signals saturate with increasing laser power), the total dye-laser power required is drastically reduced compared with the levels of Table 4. An added benefit from this change is an improved spatial resolution for the measurements.

4. NEUTRAL-HELIUM BEAM

Odajima

The neutral-helium beam is a major component of the LAPPS diagnostic system. The ion source, neutralizer, and auxiliary equipment will take up considerable space inside and outside the MTX vault.

We list below specifications of the helium-beam system, as well as other information. Figure 15 shows the basic system, including dimensions. Figure 16 shows the ion source. The source is designed for MTX by sizing the electrode set to have the same cross-sectional area as the central entrance and exit access slots. This restriction then sets the maximum ion current obtainable.

Basic Specifications

Ion beam current	0.8 A
Beam energy	50 keV
Pulse width	1 to 5 ms
Repetition time	30 s
On/Off control	On/Off of Arc Discharge
Ion species	Helium (or Hydrogen)
Neutralizer gas	Xenon

Ion Source

Bucket-type ion source.

Four filaments made from 1.2 mm tungsten wire.

Four electrodes for two-step acceleration for good focusing.

Each electrode has 42 holes of 4 mm diameter, over a total area of 20×70 mm^2.

The beam can spatially scan at the center of the MTX torus by pivoting the ion source up to ±2° with 0.1° accuracy.

The beam is focused to a 20 mm diameter at the plasma center.

Power Supplies

Power Supply for Filament	
Output	15V/400A
Pulse width	4 s
Repetition time	30 s
Ripple	Less than 5% peak-to-peak
Disconnection of filament	Detectable

Power Supply for Arc Discharge	
Output	100V/200A
Pulse width	2 to 10 ms
Repetition time	30 s
On/Off control	Made using a transistor chopper
Buildup of output power	Less than 50 μs
Power Supply for Ion Acceleration	
Condenser	50kV/3μF, 3750 J
Output	50kV/1A for 5 ms, 250 J
Voltage drop after 5 ms	Less than 10%
Charge-up time	30 s
Break down	Protected with a resistor.
Power Supply for Ion Deceleration	
Output	2kV/0.1A, constant voltage
Ripple	Less than 2% peak-to-peak

Vacuum Pumping

Turbo-molecular pump (TMP) with a rotary-mechanical-pump system.

Pumping speed is 2200 liter/s at the top of the TMP.

10-inch gate valve.

Both pumping ducts are made of 350 mm-diameter tubing.

Each pumping duct has 250 liter/s pumping speed.

Gas Injection

Helium gas is fed to the arc chamber using a piezoelectric valve.

Xenon gas is injected into the neutralizer cell by using a fast-acting electromagnetic valve.

To measure beam power and profile, two detector arrays are planned. The first is a 14-channel electrostatic analyzer (Faraday Cup) crossed array at the top of the neutralizer. The second is a calorimeter array at the helium-beam dump in the central exit access slot.

Magnetic shields are planned so as to reduce the MTX magnetic field at the source and at the neutralizer. The shield around the source will be large and heavy, but it will be near the floor level so it should not be difficult to support. Calculations will be performed to determine the effect of these shields on the magnetic field at the plasma.

We plan to place the two large power supplies for the helium beam outside the south wall of the MTX vault, approximately as shown in Fig. 2. One of the two cabinets provides high voltage and power for the filament and arc of the ion source, and the other is for the accel and

decel components. The distance from a spot on the floor directly under the MTX C-port to just outside the south concrete wall along the route shown in Fig. 2 is about 8 meters. The cables will be placed in a protective covering and laid directly on the floor. Their route is shown in Fig. 2. Most of the run will be against the base of the racks for the pellet injector. A hole will be drilled in the south wall near floor level for the cables.

Remote-control racks for these power supplies will be located in the MTX control room, connected to the supplies and controllers by a fiber-optic link. A remote television camera is planned for reading the power-supply meters from the control room.

The water-cooling unit for the helium-beam source will be located outside the vault near the power supplies, and the vacuum-control rack will be placed inside the vault near the source.

5. LASER SYSTEM

5.1 Laser Specifications

Mizuno, Nilson

In LAPPS, a tunable dye laser will be used to pump the helium atoms entering the plasma from below. Methods of exciting the dye laser include: (1) Flash-lamp excitation, (2) Excimer excitation, and (3) Nd:YAG laser excitation. Possible candidates for the dye-laser system are listed in Table 5. All cover the wavelength band that includes the excitation schemes suggested in Sec. 2, from about 380 nm to 510 nm.

One requirement for the laser system chosen is that it should be applicable to both the allowed-line-excitation and the forbidden-line-excitation types of measurement schemes. A qualitative comparison of the pulse-length and laser-power requirements is shown in Table 6.

However, the requirements addressed in Table 6 are not the only requirements. For example, we need a long laser pulse for various reasons. For measurements of the electric field of an electron-heating beam produced by a gyrotron, an electric field low in comparison with that of an FEL beam, we will need a long measurement time (up to 500 ns) because of the expected low signal levels. Even for the measurements of the electric field of the FEL beam, with its projected pulse length of 20 to 50 ns, it is preferable for the dye-laser pulse to be at least up to twice as long. Then, the laser beam can be present before, during, and after the FEL pulse so that the effect of the FEL electric field can be clearly demonstrated. Also, if we were to use a flashlamp laser, which can have a jitter in the laser timing of as much as 100 ns, an even wider laser pulse is required to insure that it will encompass the FEL pulse.

We now comment on each of the excitation schemes in Table 5, in inverse order of their listing in the table.

The Nd:YAG laser of Quantel International is a reliable high-power laser. However, the pulse width of the laser is short (<10 ns), so that the detected signals may be 1/5 of the values estimated in Sec. 3 (where a 50-ns laser pulse is assumed). This might be acceptable for the forbidden-line-excitation schemes, but not for the allowed-line excitation schemes.

An excimer-excitation laser is reasonably reliable. It is claimed that laser (2-a) in Table 5, a newer eximer laser produced by Lambda Physik, is reliable. This laser has a rated output energy of 20 mJ and a pulse width of 50 ns. It satisfies both requirements of high power for forbidden-line schemes and of long pulse length for the allowed-line schemes.

The second excimer-excitation laser listed in Table 5 (2-b) is presently on hand at JAERI and is available for use. This laser is certainly appropriate for performing the checkout and calibration experiments at JAERI, and it probably can be use for FEL electric-field measurements if the timing of the laser and FEL can be properly synchronized. The pulse length of this laser is about 25 ns, so that the estimated number of photoelectrons will be about half the values given in Table 4 for the power levels listed there. This will be no problem for the forbidden-line-excitation scheme, where a strong signal is expected. Allowed-line-excitation schemes produce relatively weak signals, so that the reduction of the factor of two is of concern.

The flash-lamp-excitation laser [(1) in Table 5] claims output power of >1 MW, spread over a long pulse (500 ns). The reliability of such a laser at high power output needs to be checked. This laser will be appropriate for the allowed-line-excitation schemes because only low power is required there. If the reliability is less at high output power, this could be a matter of concern for the forbidden-line-excitation schemes. However, if the LAPPS helium beam has a high enough intensity, our recent calculations of forbidden-line excitations suggest that higher level excitations of the triplet metastable state, and also of the singlet, will produce significant signals. For these alternatives of the forbidden-line-excitation schemes, high laser power is not required. Thus any lack of reliability at high power levels may not be important.

We are continuing our investigation of available laser systems for LAPPS. If the laser we presently have available at JAERI operates reliably, we plan to start with it. If necessary, we can double its pulse length by using a two-path system, with a 25-ns delay in one path. We will lose one-half the energy with this scheme, though. Later, if we decide we need the long duration of a flash-laser pulse, we may purchase a laser such as item (1) in Table 5.

5.2 Laser Transport System — Nilson

We intend to locate the dye-laser system in a room just outside the MTX vault (see Figs. 2 and 17). The room will be equipped with the necessary hazard controls for a Class 3 laser system. We are currently working with the LLNL Hazards Control Department to determine exactly what these controls will be. It is certain that the beam must be completely enclosed during high-power operation, especially in the vault area. Further safety controls will include interlocks to the laser room, access doors, and beam-tube shutters. We will be adhering to the ANSI laser safety standards for this installation.

If we should use an excimer laser with HCl gas, we will have to determine the maximum amount of gas that could leak from the supply bottle and design the appropriate gas handling system. This could involve placing the supply bottle in a gas cabinet located outside the laser building.

The laser transport system consists of a series of six turning-mirror boxes and beam pipes (see Fig. 17). The first four turning mirrors will be mounted on the west wall of the MTX vault area. These are concrete walls ranging from 12 to 72 inches (30 to 180 cm) thick, which should be extremely stable. There are a number of liquid-nitrogen pipes and power-supply trays that must be avoided as the beam tubes traverse the west vault wall. Therefore, a close interaction between LLNL and JAERI during the design phase of the transport system will be required to avoid interferences. The final two mirrors and focusing optics are mounted on the MTX machine and JAERI entrance box (Fig. 18), which may move relative to the concrete walls when the magnetic field is turned on. During the next MTX run, we will measure the wall and machine vibration levels to ensure they are sufficiently stable. Depending on the amount of beam divergence that we encounter, and on the control needed over the size and shape of the laser beam at the plasma, additional relay lenses may be required and are being considered.

Figure 18 shows the path of the laser beam from its entrance at the JAERI box to the plasma. Any optical components inside the vacuum must be kept well out of the FEL beam. Here, we may need a prism to shift the laser beam up so as to miss the bellows between the JAERI box and the main MTX machine.

For alignment purposes, we place a beam-splitting cube viewed by a camera into the beam path just before the fifth turning mirror. This will provide a viewing path both back along the transport system and towards the tokamak. Using this viewing camera and the final two turning mirrors, we will align the transport system to a crosshair at the JAERI entrance box and reference marker located on the inside wall of the tokamak. See Sec. 6 for further discussion of the alignment procedure.

We expect the transport system to use 2-inch (5.1-cm) diameter turning mirrors and beam tubes. It would be preferable to use an automatic alignment sensor with remote-control crosshairs and mirrors to enable one person to align the system. Verification of the alignment could then be done from the control room. Automatic sensor boxes that include mirrors and cross hairs are used in the LLNL laser program and would be available for reference during the design of the transport system.

It would be prudent to insert a separate low power visible alignment laser into the laser beam path back in the laser room. This would greatly facilitate manual alignment of this system out in the vault area without adding significant laser hazards.

6. DETECTION SYSTEM AND OVERALL ALIGNMENT

Nilson

6.1 Detection System

We have completed a layout of a possible configuration for the collection optics for LAPPS (see Fig. 19). It consists of a set of mirrors, lenses, beam splitters, and wavelength filters placed inside the port access cylinder on the top MTX C-port. First, the optical signal from the interaction region between the FEL, plasma, laser, and neutral beam reflects off mirrors that are placed in the inner and outer slots of the top C-port. The light through each slot then passes through a vacuum window on the bottom of the port cylinder, where a lens then collects and collimates it. The collimated light from each slot is then separated into two beams by a dichroic mirror before it is filtered and focused onto two photomultiplier (PM) detectors. (Some measurement schemes discussed in Sec. 2 require the detection of two wavelengths, while other schemes require the detection of only one wavelength.) We align the two sets of beams so that the coplanar signals from each slot intersect each other at the detector plane, thus requiring only one detector for each wavelength.

As shown in Fig. 19, there are three access slots at the top C-port. The central slot will contain a beam dump to absorb the power of the helium beam coming through the bottom C-port. We use both upper side slots for collecting light from the plasma region to double the detected low signal levels.

In the detector location shown in Fig. 19, the magnetic field is expected to be 2500 Gauss. This may require a large magnetic shield to decrease the field at the PM tubes to as low as 0.5 Gauss, as specified by the detector manufacturer. We are considering adding an optical relay system just before the detector to transfer the image out of the port cylinder so that the detector can be placed in a lower magnetic field. This will decrease the amount of magnetic shielding needed around the PM tubes and also will move the tubes out into a more accessible region. Less shielding means less bulk and weight to manage and also less effect on the magnetic field at the plasma. Although in this section we discuss the arrangement shown in Fig. 19, the option of moving the PM tubes further out of the cylinder is being considered. We are also investigating how we can increase the space around the

detectors by either tilting the dichroic mirror or adding optics to reduce the image and detector size.

Wherever the location of the PM tubes, the entire optical system must be within a light-tight enclosure and we need to regularly check the calibration of the PM tubes. A calibration source (A) and insertable mirrors (D) are shown in Fig. 19, to be used for checking the gains of the PM tubes and electronics that follow. We may use a quartz lamp for the calibration-light source.

Figure 20 shows a cross section of the collection optics mounted inside the port cylinder. Two rotation stages and one translation stage are mounted to the side of the beam-splitter housing for alignment purposes. The two rotation stages provide pitch and yaw motion while the translation stage allows the housing to adjust the viewing region ±3 cm along the FEL beam line, with 2-cm spatial resolution. One must be aware of the disproportionate response that the two exiting beams will have to the pitch and yaw adjustments. The unsplit (straight-through) beam from the dichroic mirror will see little effect from the rotation and goniometer adjustments, while the split beam exit angle will have a linear response to these motions. The proposed alignment procedure for the housing is discussed in Sec. 6.2.

Although the alignment stages could be operated using a long tool through the open end of the cylinder, it would be best if they are remotely driven with either motors or flexible shafts from outside the cylinder. This would help eliminate the possibility of accidental misalignment. The three stages and their respective mounting positions shown in Fig. 20 may not be the most optimum units to use. Furthermore, a more detailed ray trace may show that the required ranges of travel may change slightly.

We are also investigating possible glass-to-metal sealing techniques that could be used on the vacuum windows at the bottom of the port cylinder (see Fig. 19). Most manufacturers of these seals require that the sealing surface be circular in shape. This circular shape is still possible with our design; however there is little room for sealing material between the extreme left and right edges of the windows and the sides of the cylinder. This limited space will most likely eliminate the possibility of using removable windows. We show a possible quartz-to-metal seal configuration in Fig. 21, and are

currently reviewing other possible sealing techniques.

A possible mirror-mounting technique could emulate a method that has been used for signal-cable support inside the C-port slot. It consists of two wedged pieces that are forced against the slot wall as its center clamping screw is tightened. Flat locating edges on these mounting pieces could align the mirror to the sides of the slots. We feel it will be unnecessary to provide tilting adjustments for each mirror as the beam-splitter housing and detector mounts will have sufficient alignment adjustments.

We have investigated possible anti-reflection and high-reflection coatings for the laser transport and collection optics and have found that all of the required coatings are commercially available.

To keep the alignment uncertainties to a minimum, it is prudent to incorporate an insertable alignment ball into this diagnostic system. This would allow a daily alignment check to be made of the laser beam, neutral beam, and collection optics. We propose using a glass ball attached to the end of an optical fiber that emits the appropriate signal wavelength, thus allowing the collection optics to be calibrated on a daily basis. A possible insertion method for this ball is shown in Fig. 22. One of the important design constraints is that the ball must fully retract into the bottom side slot after use. Additionally, the ball must be able to move ±3 cm along the FEL beam axis for scanning purposes. Finally, one must address space-allocation issues associated with the large number of items that must have a vacuum interface through the bottom of the C-port. These include the neutral beam (6-inch-OD flange), calorimeter signal cables (3 2.75-inch-OD flanges), microwave waveguide (2.75-inch-OD flange), alignment-ball fiber (2.75-inch-OD flange), and any possible alignment-ball drive mechanisms.

6.2 Overall Alignment

The neutral beam, laser beam, and the collection optics might be aligned using the following procedure:

(1) Begin by establishing a north/south and up/down reference marker for the laser on the inside wall of the tokamak (see Fig. 17).

(2) Again, while the machine is at air, the east/west positioning of the alignment ball must be calibrated using the center slots.

(3) Align the laser system up to the viewing camera and through a final cross hair at the opening to the JAERI box. Using the viewing camera in conjunction with mirror M6, we then align the laser to the reference marker on the inside wall of the tokamak.

(4) Run the alignment ball up to its center position using the viewing-camera cross hairs as a reference.

(5) With the alignment ball in place, the neutral beam can be aligned using a temporary telescope that is centered on the alignment ball and on the middle slot of the upper C-port. Further neutral-beam alignment must be done actively with a thermistor array.

(6) Finally, the collection optics can be aligned by first removing the beam-splitter housing and setting reference markers for the two image points where the detectors are to be placed. This can be done by placing cross hairs in the center of the port cylinder at the appropriate distances from the vacuum windows.

(7) A telescope should be used to establish a line of sight between these reference markers and the alignment ball while the machine is at vacuum.

(8) It must then be determined that the slot is centered on this line of sight. If it is grossly misaligned, then the mirrors inside the tokamak must be adjusted at air so that everything is colinear.

(9) The beam-splitter housings can then be inserted. This should be done with the interference filters in place. However, because one of the forbidden-excitation schemes requires UV light, it would be difficult to view the alignment ball images. If possible, a fluorescent card can be used to aid in viewing these images. The housings can now be adjusted using the translation stage so that the first two image points are centered again on the reference marker. Then, by adjusting the pitch and yaw of the housing, the two new images from the beam splitter can be placed at points directly above the first reference points. As previously discussed, the first two beams should be very insensitive to the pitch and yaw motions when aligning the final two images.

(10) The two detectors can now be placed at their reference markers and locked into position. The housings must be aligned using the

detectors as discussed in step 11.

(11) Subsequent daily alignment of the neutral-helium and laser beams can now be done repeating steps 3-5. This can be done by placing a small aperture in front of the detector and adjusting the beam-splitter housing until the straight-through signal from the alignment ball for each housing is maximized. This process is then continued for the corresponding signals from each beam splitter.

7. DATA ACQUISITION: ELECTRONICS AND COMPUTERS

Casper

The LAPPS diagnostic will require the acquisition of up to four channels of data. In the allowed-line-excitation technique (see Table 2), measurement of light emission from the plasma using PM tubes is required for both the allowed and forbidden (FEL induced) line transitions. The proposed forbidden-line-excitation scheme requires only a measurement of the increase in emission from an allowed line (one PM tube), emission enhanced by pumping through a forbidden line. In addition to the up-to-two PM tube signals, it is desirable to measure the input laser light. The fourth channel can record a signal derived from the FEL beam, for example. In this way, the timing of the LAPPS system can be synchronized with the FEL and documented by the recorded data.

For this diagnostic instrument to be capable of measuring microwave electric-field strengths from a pulsed FEL, it must be able to resolve temporal variations on the scale of a single FEL pulse, whose duration is 10 to 50 ns. For good temporal resolution of the FEL pulse, it would be advantageous to use digitizers with sampling rates of ≈1 GHz, with nominally 8 bits of accuracy.

The duration of recorded data must be sufficient to observe the emitted light before, during, and after the FEL pulse so as to measure changes induced by the pulse. In addition, sufficient duration is required to observe multiple pulses and to provide the capability for averaging over several pulses. Professor Oda has requested that averaging over samples be provided in the software portion of the acquisition system.

These data sampling and storage requirements can be met either with a LeCroy 7242 digitizing oscilloscope as proposed by the JAERI group or with additional channels of Analytek digital recorders, an instrument that is presently in use on the MTX project. Both of these recorders have storage of 50 kilowords/channel, which should provide for a sufficient acquisition duration (e.g., 50 μs at 1 GHz, or over a longer period in burst mode). The final selection will be determined later.

Computer acquisition of the four data channels will be accomplished with the HP-UX computer supplied by JAERI and presently used by

Dr. T. Ogawa at LLNL for acquisition and analysis of his fast neutron measurements. This computer has sufficient capability to satisfy the requirements of both LAPPS and the neutron measurements. The location of this computer is in the MTX control room. It is connected to the neutron diagnostic CAMAC crate using a fiber-optical HPIB extender.

At the present time, it is uncertain where the digitizers for the LAPPS diagnostic are to be located. Possibly they will be installed in the MTX control room in order to utilize their many features. This will require additional definition and engineering design to insure proper ground and voltage isolation from the MTX tokamak while preserving the high-frequency response in the required signal conditioning and buffering between the MTX vault and the control room. To avoid these problems, we may decide to install the digitizers in the MTX vault near the tokamak machine.

Use of the above-mentioned digitizers will require additional development of the HP-UX data-acquisition system because neither unit is presently in use in this portion of the MTX acquisition system (this would also be true of direct acquisition into the VAX computer). This development can be supported in whole or in part by the LLNL group but the full scope of this work must yet be discussed and defined. This area will be included in further discussions of the LAPPS diagnostic, along with discussions of the detection electronics and the integration into the MTX timing system. Archiving of the data to tape by the VAX is provided by the MTX computer system in our standard manner for a UNIX acquisition subsystem.

Many of the data-analysis software routines are to be supplied by Professor Oda. Some reprogramming may be necessary for the computers available on the MTX project. This can be accomplished either on the HP-UX or VAX computer system. In either case, MTX will supply the programming support as is needed.

8. OTHER POSSIBLE DIAGNOSTIC APPLICATIONS

Allen

The LAPPS diagnostic system consists of a laser, a neutral-helium beam, and a high-efficiency detection system. To date, there have been very few (if any) high-toroidal-field, high-density experiments that have had either neutral-beam heating or a diagnostic neutral beam. The LAPPS neutral-helium beam possibly provides unique diagnostic possibilities if there is enough signal to allow measurements.

The most interesting application would be a charge-exchange-recombination (CXR) measurement of the ion temperature. Either ionized helium or an impurity such as CVI is recombined with the neutral-helium beam. From the Doppler width of the emitted light, one obtains the local ion temperature. This is a standard diagnostic on machines such as DIII-D that employ neutral-beam heating. By adding to the LAPPS apparatus several channels detecting different wavelengths, we may be able to obtain an estimate of the ion-temperature profile. Needless to say, ion-temperature profiles in a high-density, high-magnetic-field tokamak are very important, particularly in conjunction with some of the recent work with ion-temperature gradient modes. Previous measurements on Alcator-C used the Doppler width of several intrinsic emission lines; a radially resolved measurement with CXR, particularly during pellet experiments, would provide new physics information.

Discussions have begun with the JFT-2M group to estimate the intensity of the CXR emissions. We have already estimated that the attenuation of the neutral-helium beam in the MTX plasma will be about 40 % to 60 % (i.e., from the edge of the plasma to the center at an average density of 1×10^{14} cm^{-3}). This means that the on-axis neutral-helium equivalent current for the LAPPS beam at the plasma center may be about 0.1 to 0.2 A. We are now trying to decide if the CXR scheme will work for MTX, based on the efficiency in the JFT-2M system, the neutral-beam current, and the amount of CVI in the plasma. The exact diagnostic configuration is still to be determined, but it might even use an insertable mirror in the JAERI box for the detection system so that radial profiles could be obtained. Future progress on this particular diagnostic hinges critically on the intensity estimates.

Yet another interesting application of primarily the helium beam is to measure fully stripped impurity densities, again using CXR. In this case, the detector system does not have to be radially resolving, but must be absolutely calibrated. A fully stripped carbon or oxygen ion is recombined with the helium beam, and the emission of light from the ion is used to determine the fully stripped impurity density. If the detection system is radially resolving, it may be possible to determine the radial profile of the fully stripped state, which provides important information on radial transport of impurities (and perhaps information on the diffusion coefficient as a function of radius).

Two other applications of the LAPPS equipment may be possible, but more calculations are necessary to determine the applicability of the techniques. The first is to use the laser beam and a detection system to measure the edge-impurity states with laser fluorescence and thereby determine the edge-impurity behavior. This technique has been used successfully in other tokamaks, and may be possible with the LAPPS system. The other technique is to use this system to measure the Zeeman splitting of a particular line and thereby estimate the radial profile of the magnetic field. This would be similar to the lithium-beam experiment performed on Alcator, but a more localized measurement would be possible if laser pumping were used. This measurement would require detection optics that could accurately measure both polarizations of the emitted light. It may be possible to incorporate this ability into the planned LAPPS detection system.

9. CONCLUDING REMARKS

Work is progressing on the various components of this microwave-electric-field diagnostic system. In parallel, physics calculations are continuing to improve our understanding of the parameters involved and to help pick the most promising spectroscopic scheme with which to begin our measurements.

The present schedule for progress on LAPPS is shown in Fig. 23.

Acknowledgements

We wish to acknowledge the early active participation in this work by Dr. E. Bickford Hooper of LLNL. The support of Dr. Hikosuke Maeda of JAERI is also greatly appreciated.

The MTX project and the participants in this work from LLNL are supported under the auspices of the U.S. Department of Energy by the Lawrence Livermore National Laboratory under Contract No. W-7405-ENG-48.

9. CONCLUDING REMARKS

Work is progressing on the various components of this microwave-electric-field diagnostic system. In parallel, physics calculations are continuing to improve our understanding of the parameters involved and to help pick the most promising spectroscopic scheme with which to begin our measurements.

The present schedule for progress on LAPPS is shown in Fig. 23.

Acknowledgements

We wish to acknowledge the early active participation in this work by Dr. E. Bickford Hooper of LLNL. The support of Dr. Hikosuke Maeda of JAERI is also greatly appreciated.

The MTX project and the participants in this work from LLNL are supported under the auspices of the U.S. Department of Energy by the Lawrence Livermore National Laboratory under Contract No. W-7405-ENG-48.

References

1. Free-Electron Laser Exeriments in Alcator C, edited by K. I. Thomassen, Lawrence Livermore National Laboratory Report PROP-00202 (1986).
2. U. Rebhan, N. J. Wiegart, and H.-J. Kunze. Phys, Lett. A85, 228 (1981).
3. U. Rebhan, J. Phys, B: At. Mol. Phys. B19, 3847 (1986).
4. K. Takiyama, K. Kadota, T. Oda, M. Hamamoto, T. Ohgo, Y. Kamiura, K. Adati, and J. Fujita, Rev. Sci. Instrum. 59, 2351 (1988).
5. K. Mizuno, T. Oda, E. B. Hooper, K. Takiyama, K. Kawasaki, and Y. Matsuda, Sixteenth IEEE International Conference on Plasma Science, p. 140, Buffalo, NY, 1989.
6. T. Oda, K. Mizuno, E. B. Hooper, Y. Matsuda, K. Takiyama, K. Kawasaki, and K. Odajima, Fourth International Symposium on Laser-Aided Plasma Diagnostics, P. 169, Fukuoka, Japan, 1989.
7. K. Mizuno, J. Foote, T. Oda, K. Takiyama, M. Shiho, K. Odajima, K. Oasa, and Y. Matsuda, Seventeenth IEEE International Conference on Plasma Science, Oakland, CA, May 1990.
8. M. Baranger and B. Mozer, Phys. Rev. 123, 25 (1961).
9. H.-J. Kunze and H. R. Griem, Phys. Rev. Lett. 21, 1068 (1968).
10. W. S. Cooper and H. Ringler, Phys. Rev. 179, 226 (1969).
11. W. W. Hicks, R. A. Hess, and W. S. Cooper, Phys. Rev. A5, 1445 (1972).
12. K. Kawasaki, K. Takiyama, and T. Oda, Jpn. J. Appl. Phys. 27, 83 (1988).
13. T. Fujimoto, J. Quant. Spectrosc. Radiat. Transfer 21, 439 (1979).
14. D. Baye and P-H Heenen, J. Phys. B6, 1255 (1973).
15. R. L. Freeman and E. M. Jones, Culham Laboratory Report CLM-R 137, May 1974.
16. E. Saltzborn, Proceedings of the Nagoya Seminar on Atomic Processes in Fusion Plasmas, IPPJ-AM-13, p. 44, Sept. 5-7, 1979.

Table 1 Personnel with responsibilities for the LAPPS diagnostic system and their institutions.

Dr. Kazuo Odajima	Japan Atomic Energy Research Institute (JAERI), Ibaraki, Japan.
Professor Toshiatsu Oda Professor Ken Takiyama	Department of Applied Physics and Chemistry, Faculty of Engineering, Hiroshima University.
Dr. Katsu Mizuno	Plasma Physics Research Institute, UC and LLNL, and University of California at Davis.
Dr. James H. Foote Mr. David G. Nilson Dr. Steven L. Allen Dr. Thomas C. Casper	Lawrence Livermore National Laboratory (LLNL), University of California (UC) and U.S. Department of Energy (USDOE).

Table 2 Possible allowed-excitation schemes for measuring electric fields with LAPPS. The HeI energy levels involved are listed.

		Allowed line	Forbidden line	Intensity ratio R (at E=100kV/cm)	Laser
singlet	(1)	$3^1P \rightarrow 2^1S$ 501.6 nm	$3^1P \rightarrow 2^1P$ 663.2 nm	0.17	$2^1S \rightarrow 3^1P$ 501.6 nm
	(2)	$4^1P \rightarrow 2^1S$ 396.5 nm	$4^1P \rightarrow 2^1P$ 491.1 nm	2	$2^1S \rightarrow 4^1P$ 396.5 nm
triplet	(3)	$4^3P \rightarrow 2^3S$ 318.8 nm	$4^3P \rightarrow 2^3P$ 451.9 nm	0.3	$2^3P \rightarrow 4^3D$ 447.1 nm
	(4)	$5^3P \rightarrow 2^3S$ 294.5 nm	$5^3P \rightarrow 2^3P$ 404.5 nm	1.5	$2^3P \rightarrow 5^3D$ 402.6 nm

Table 3 Possible forbidden-excitation schemes for measuring electric fields with LAPPS. The HeI energy levels involved are listed.

		Allowed	Laser
singlet	(5)	$3^1D \rightarrow 2^1P$ 667.8 nm	$2^1S \rightarrow 3^1D$ 504.2 nm
triplet	(6)	$3^3D \rightarrow 2^3P$ 587.6 nm	$2^3S \rightarrow 3^3D$ 381.0 nm

Table 4 Summary of numerical results for the six cases of Tables 2 and 3, for applied electric field of 100 kV/cm.

	(a)	S_{el} (cm^{-3}) PIEL	LIF	[I_L] (kW/cm^2)	V_{obs} (cm^3) (2cm X 2cm X 5cm)	Total photo-electron (in 50 ns)
(1) 3^1P-3^1D mixing	F	1.2	0.9	[5]	20	42
	A	7.4	5.4		20	256
(2) 4^1P-4^1D mixing	F	1.5	1.2	[40]	20	54
	A	0.8	0.6		20	28
(3) 4^3P-4^3D mixing	F	2.1	3.2	[10]	20	106
	A	7.0	10.8		20	356
(4) 5^3P-5^3D mixing	F	1.1	3.2	[10]	20	86
	A	0.7	2.2		20	58
(5) 3^1P-3^1D mixing	FIF	-	69	[100]	20	1380
	b.g.	48			20	960
(6) 3^3P-3^3D mixing	FIF	−	622	[4000]	20	12440
	b.g.	487			20	9740
Brems-strahlung			0.37 (cm^{-3}/10Å)		300	111

(a) F: forbidden line, A: allowed line, FIF: field induced fluorescence.

Table 5 Possible dye-laser systems for LAPPS.

(1) Flash-lamp excitation

DL-2100B by PHASE-R Corporation

Rated output energy	3	J
Peak power	5	MW at 590 nm
	1-2	MW at 380 nm
Pulse width	500	ns
Cost	$29,150	

(2) Excimer excitation

(a) LPX 605i CC Excimer and FL 3002 Dye Laser System

Rated output energy	20	mJ
Pulse width (FWHM)	50	ns
Power	0.4	MW
Cost	$85,600 + $33,250	

(b) EMG 201 MSC Excimer and FL 3002 Dye Laser System

Excimer output energy	300	mJ
Rated output energy	30-45	mJ
Pulse width	25	ns
Power	>1	MW
(available at JAERI)		

(c) LPX 105i (Low repetition rate)

Excimer output energy	200	mJ
Rated output energy	20-30	mJ
Pulse width	20	ns
Power	1	MW
Laser medium -- XeCl		
Cost (total system)	$74,750	

(3) Nd:YAG Laser excitation

Quantel International

Rated output energy	100	mJ
Peak power	10	MW
Pulse width	<10	ns
Cost (total system)	$100,000	

Table 6 Requirements for the laser system.

Excitation Scheme	Pulse Length	Laser Power
Allowed-line excitation	Long	Need not be high
Forbidden-line excitation	Need not be long	High
Forbidden-line excitation (Alternatives)	Need not be long	Need not be high

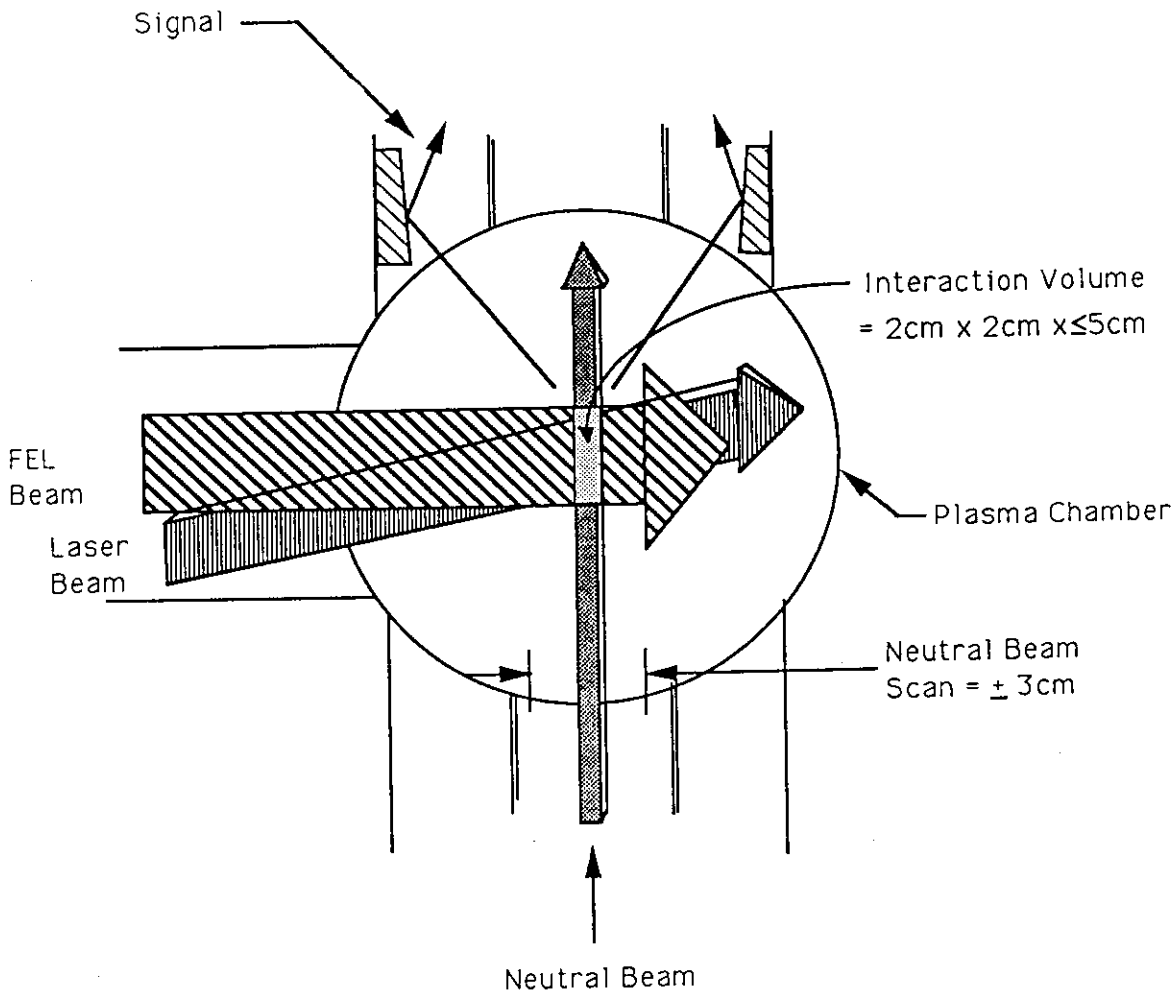

Fig. 1 Schematic drawing of the interaction region for the LAPPS diagnostic. Depicted are: (1) the plasma chamber, (2) the FEL, laser, and neutral-helium beams, and (3) the emitted light signals that are detected.

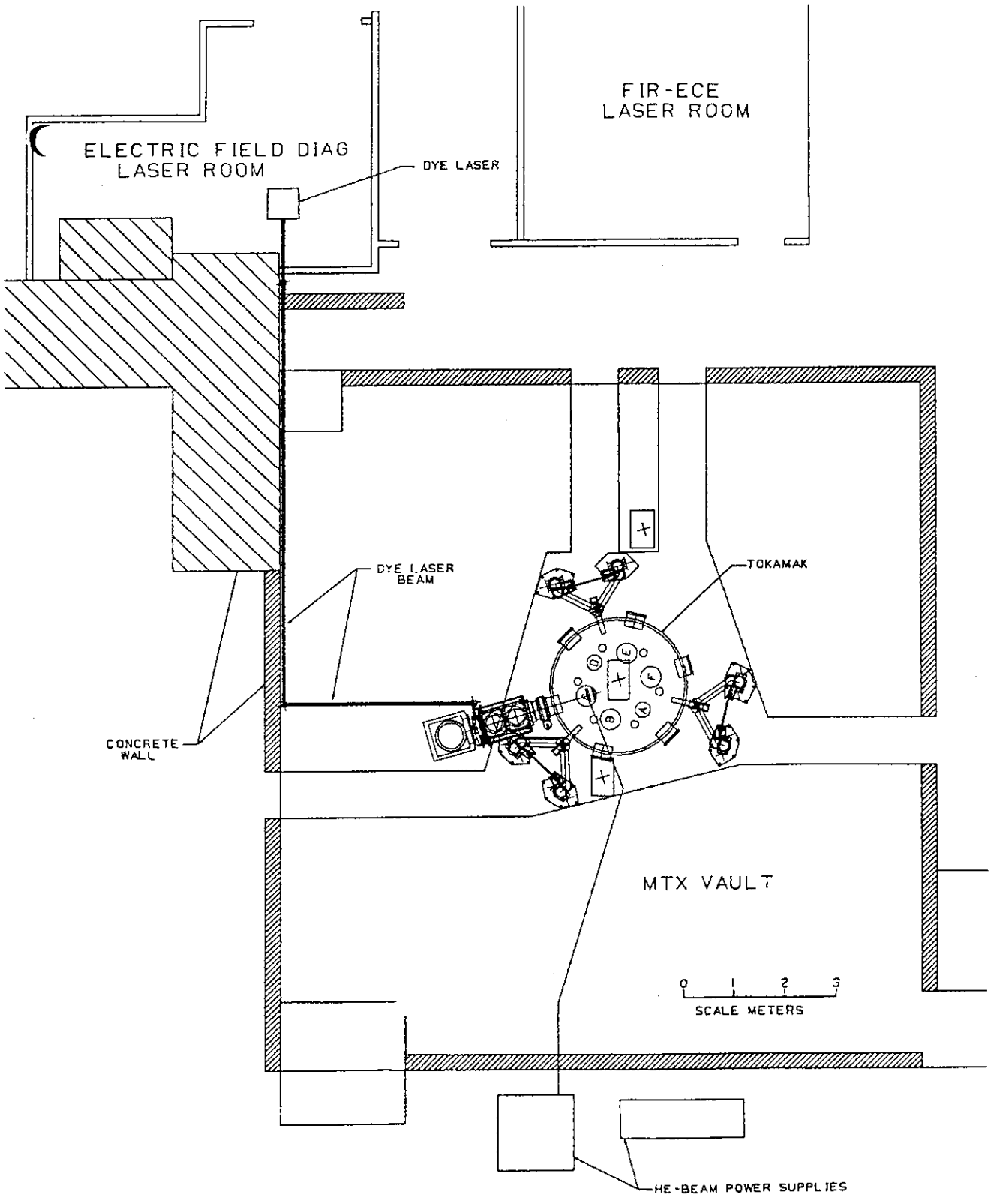

Fig. 2 Drawing of the MTX tokamak and enclosed vault area, showing placement of the LAPPS dye laser, the laser-beam transport system, and the helium-beam power supplies and cable run. The helium-beam source is directly under MTX region C, while the viewing-optics system is directly above.

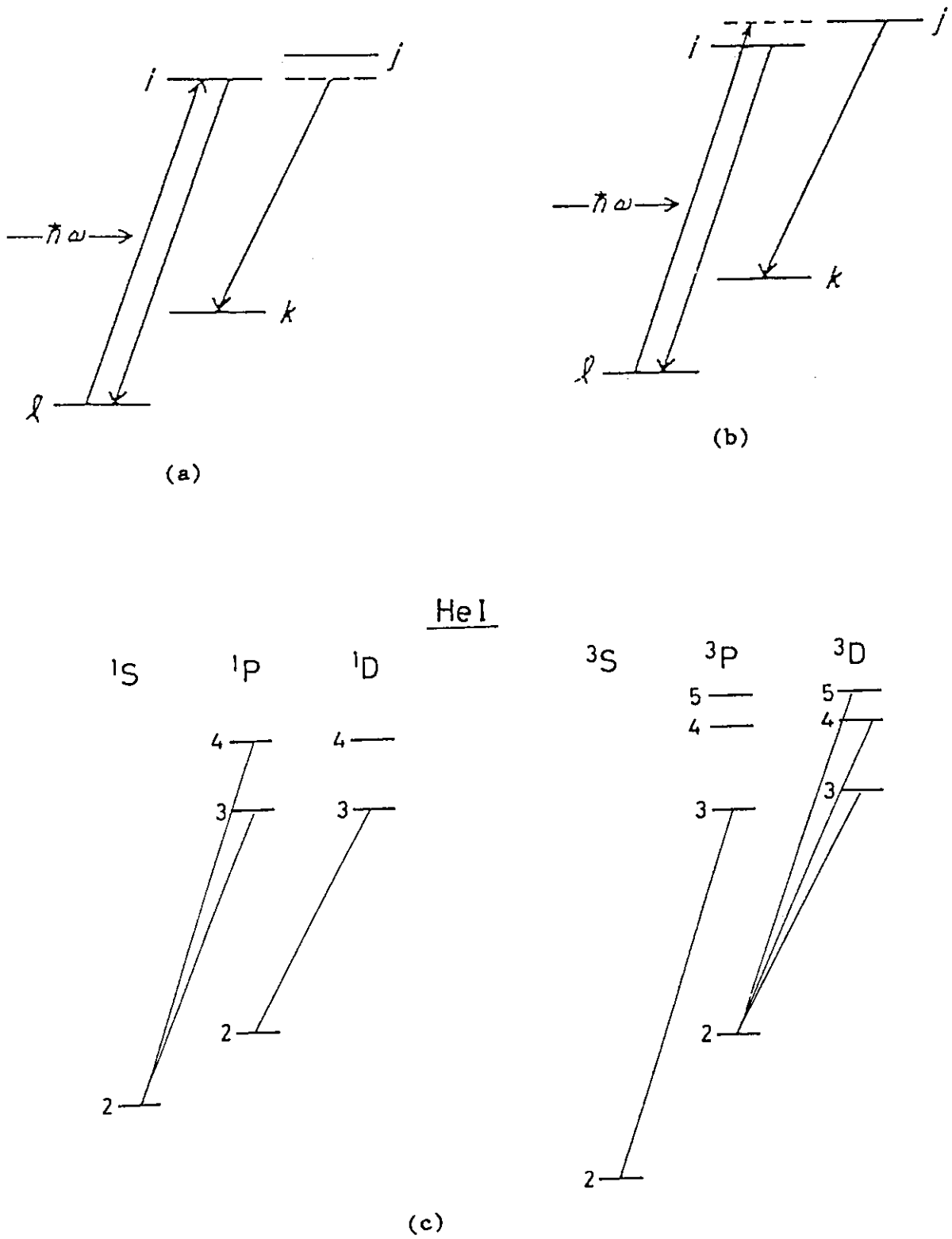

Fig. 3 (a) Energy diagram of the four-level "allowed-excitation" system developed for measuring static or quasistatic electric fields.
(b) Energy diagram of the "forbidden-excitation" system for measuring electric fields.
(c) Partial energy-level diagram of HeI, showing levels pertinent to the LAPPS measurements.

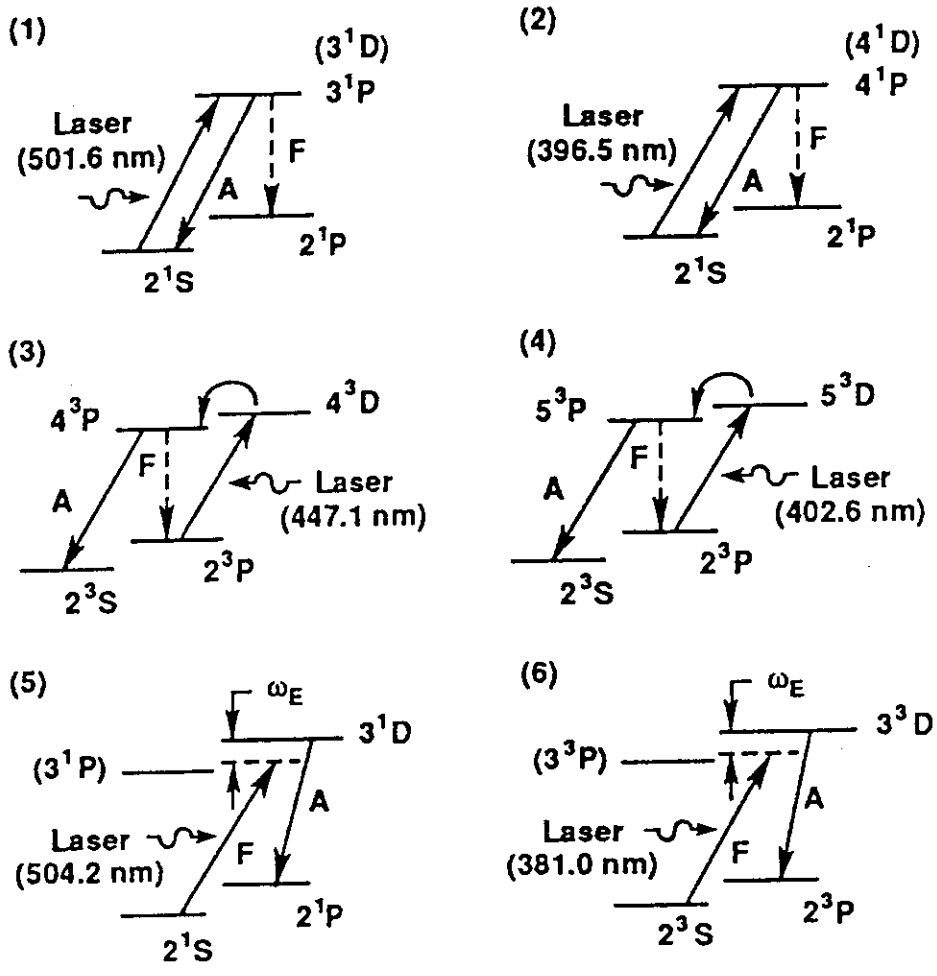

Fig. 4 Energy-level diagrams for six schemes that might be used on MTX for measuring electric fields (see Tables 2 and 3). Shown are the laser-excitation transitions and the transitions that give the emitted light to be detected. Symbols A and F designate the allowed and forbidden transitions. The diagrams for schemes (5) and (6) show an energy gap labeled with ω_E, the FEL frequency, to emphasize that a two-photon transition occurs. In schemes (1) through (4), the F spectral line is split by $\pm\omega_E$. In schemes (3) and (4), the curved arrows between the upper levels indicate transitions arising from collisional processes.

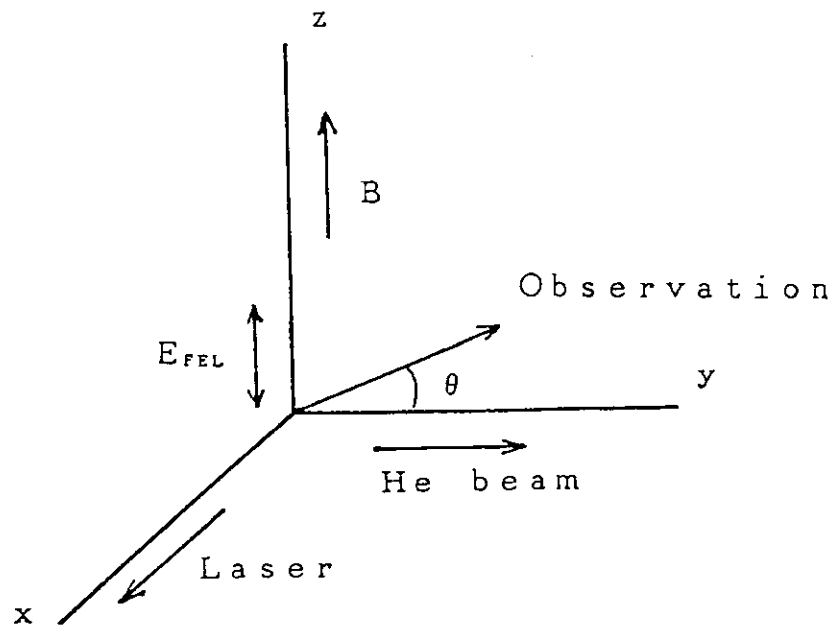

Fig. 5 Configuration for the LAPPS measurements showing the relationship of the FEL electric field, the MTX magnetic field, the helium and laser beams, and the direction of observation.

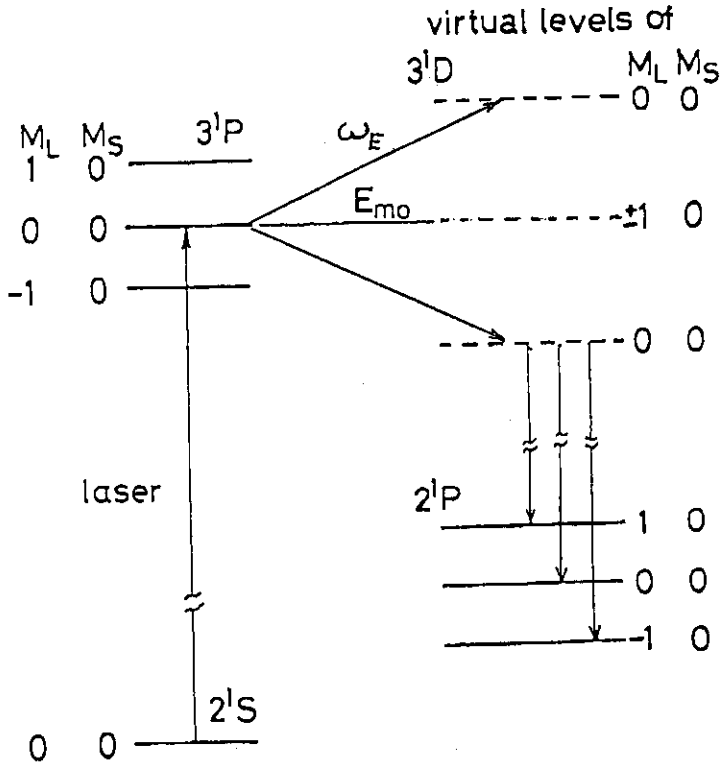

Fig. 6 Example of the Zeeman effect combined with the motional Stark effect and high-frequency effects, for the singlet energy-level system.

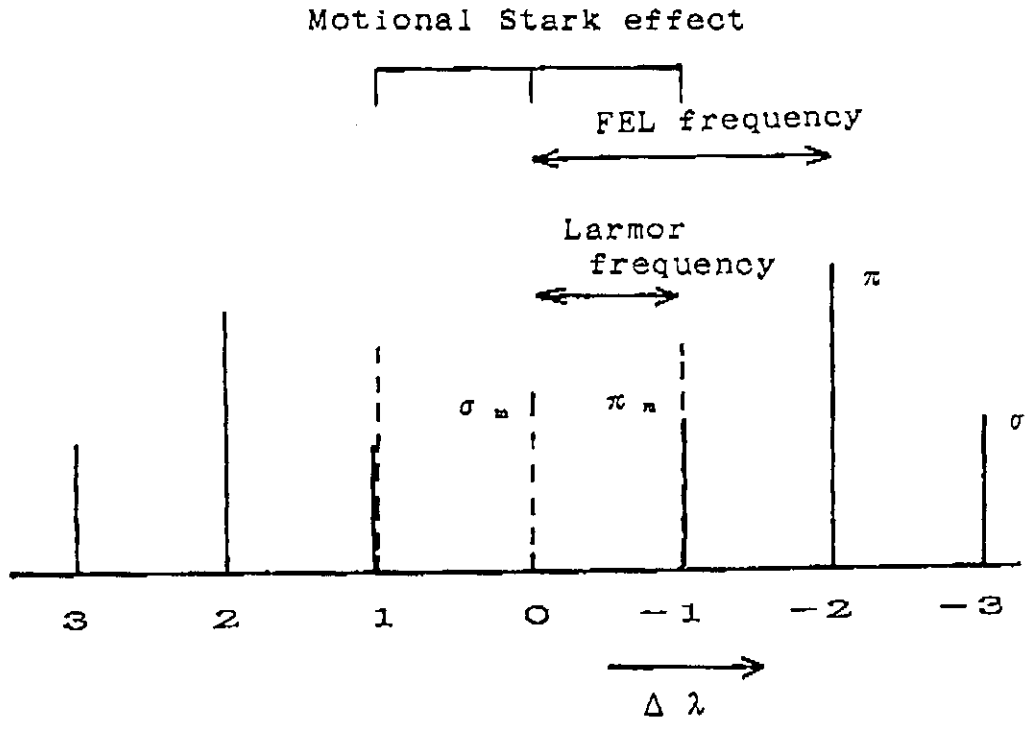

Fig. 7 Line spectrum resulting from the energy-level system of Fig. 6.

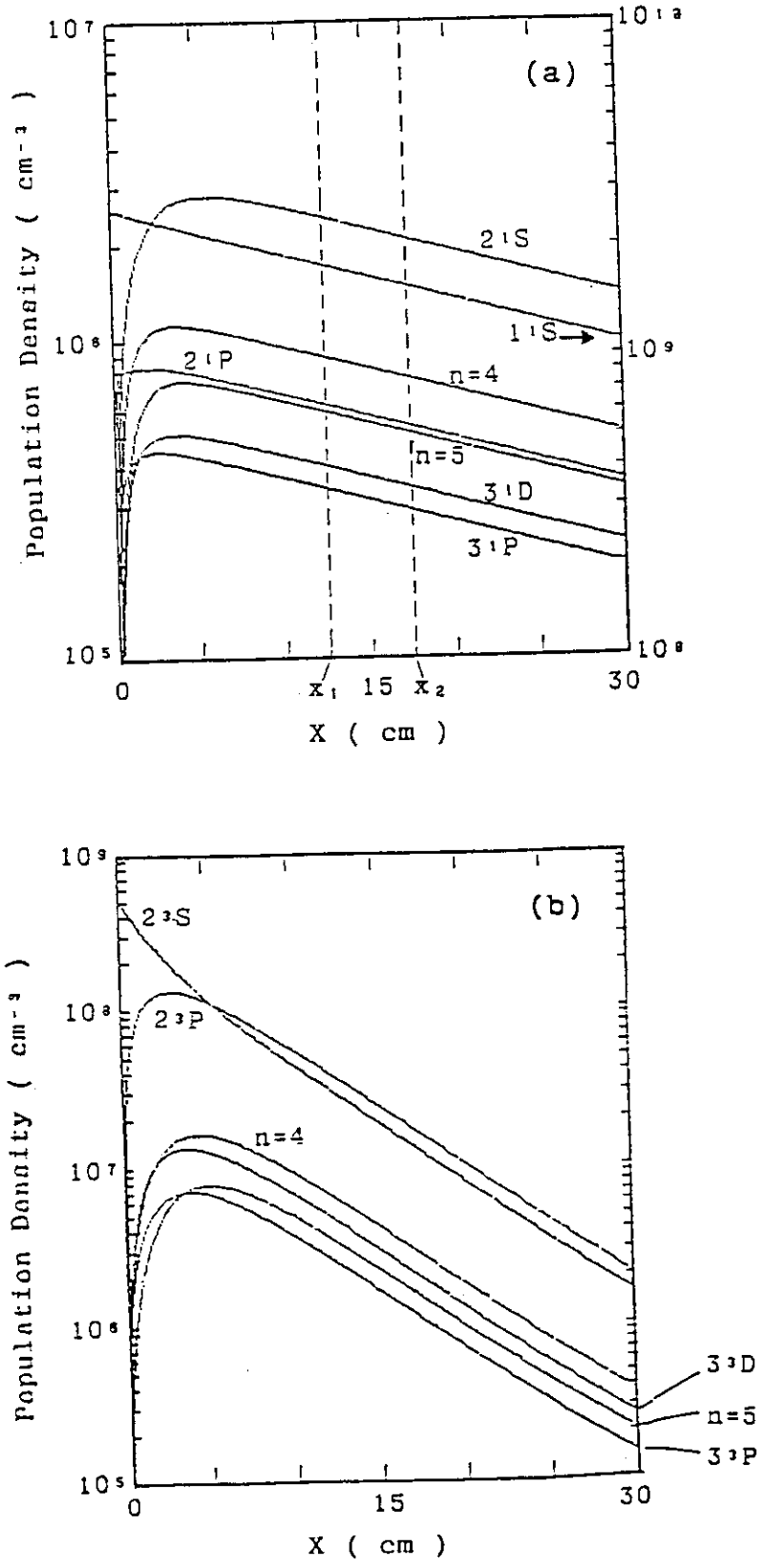

Fig. 8 Calculated spatial distribution vs position through the plasma of population densities of HeI energy levels for (a) singlet levels and (b) triplet levels. The plasma region between x1 and x2 is the location assumed in the subsequent calculations for the electric field and laser beam (x = 15 cm is the plasma center, with edges at x = 0 and 30 cm).

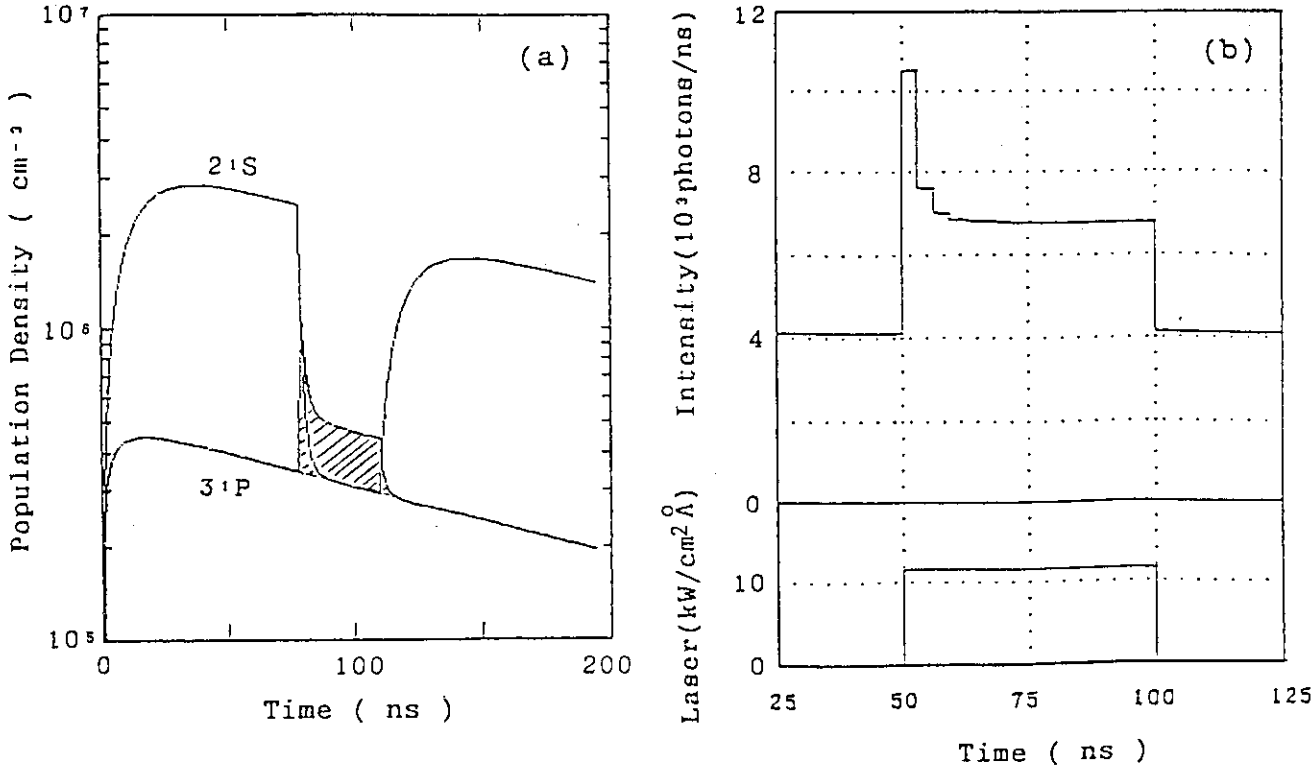

Fig. 9 (a) Calculated population densities for the HeI 2'S and 3'P energy levels for allowed-excitation Case (1) of Table 2 and Fig. 4 as a function of time during helium-beam passage through the MTX plasma with laser excitation near the plasma center. The hatched area for level 3'P is discussed in Appendix 2.

(b) Upper -- the calculated rate of photon emission vs time from a unit volume within the observation region along the helium-beam path through the plasma. Lower -- laser power profile used in the calculation.

(c) Number of emitted photons vs laser power originating from LIF (laser-induced fluorescence) and the sum of LIF and PIEL (plasma-induced emission light).

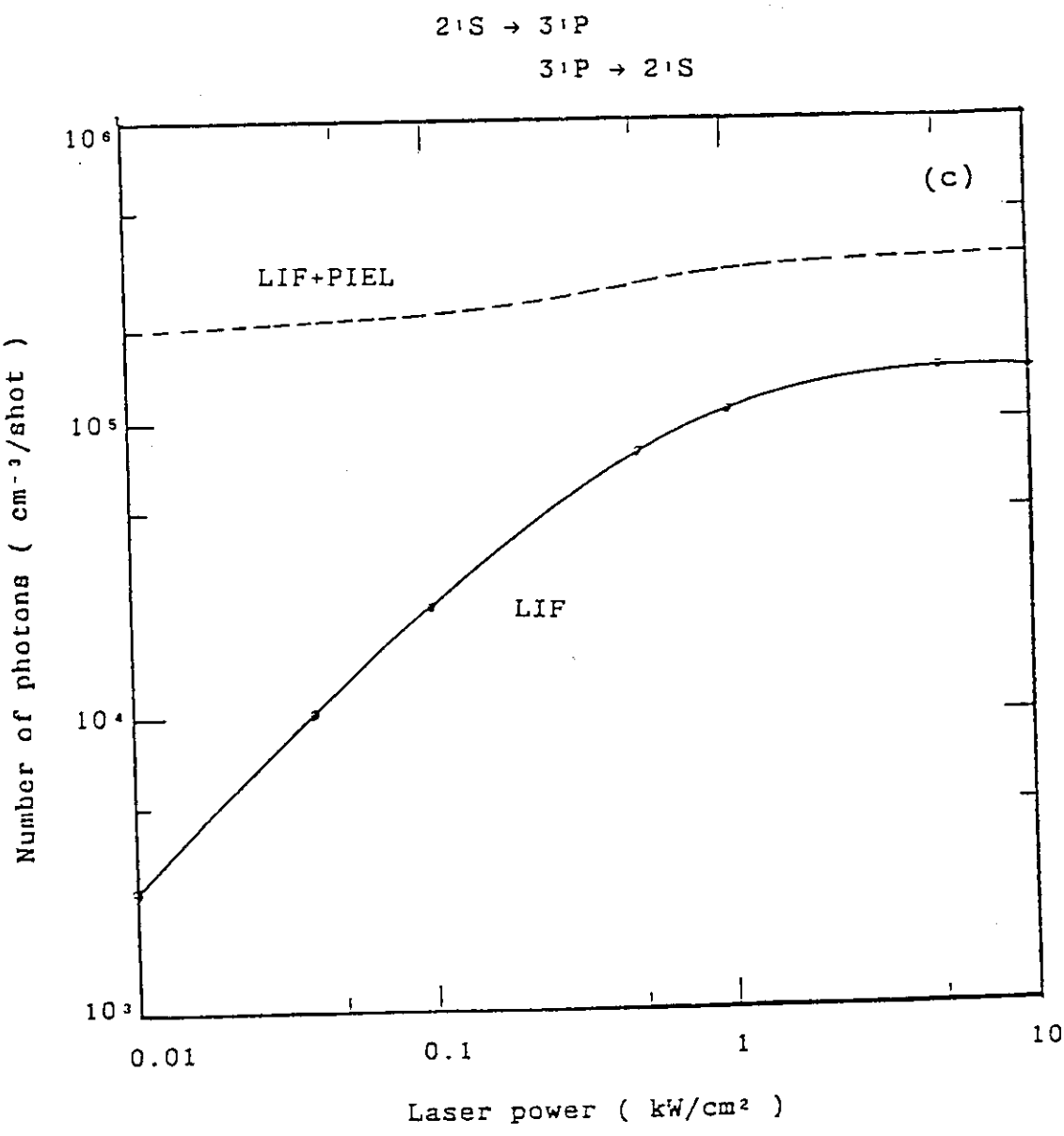

Fig. 9 (Continued)

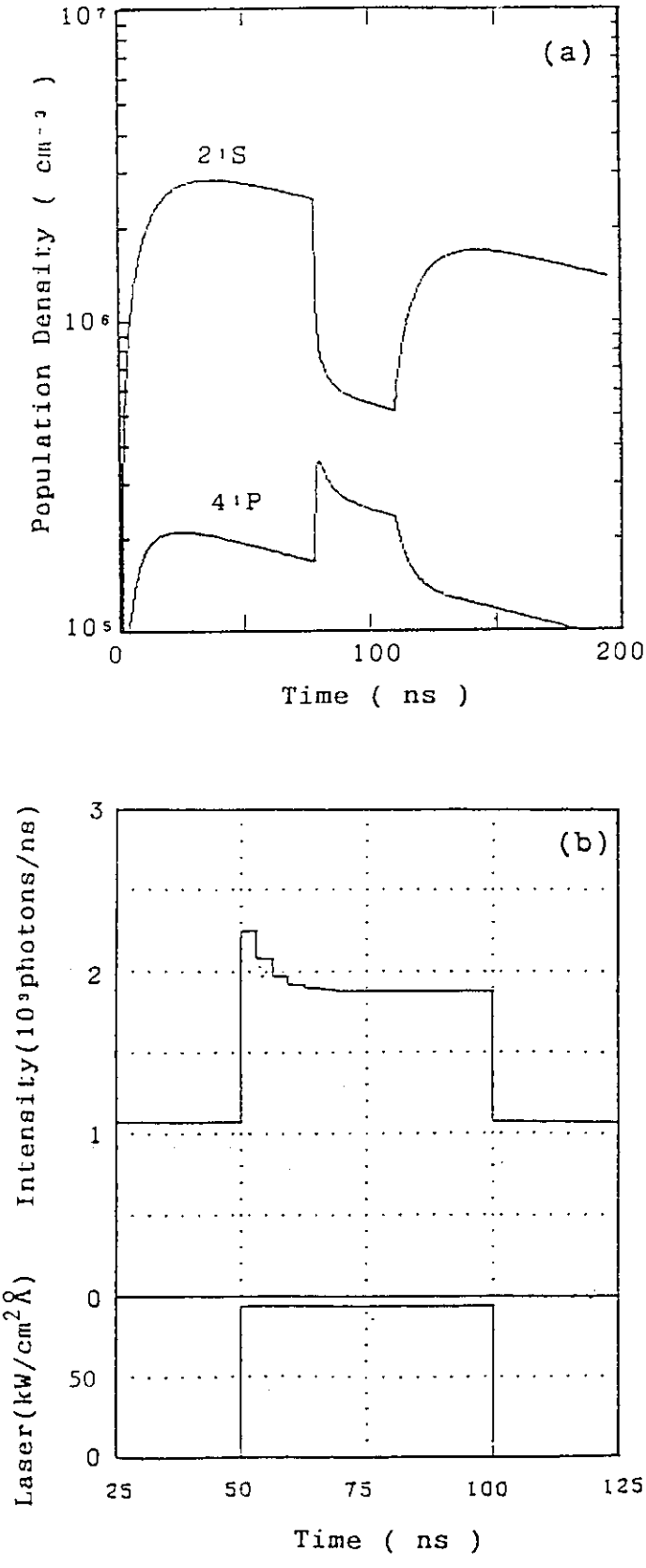

Fig. 10 Same as Fig. 9 except now for Case (2) of Table 2 and Fig. 4.

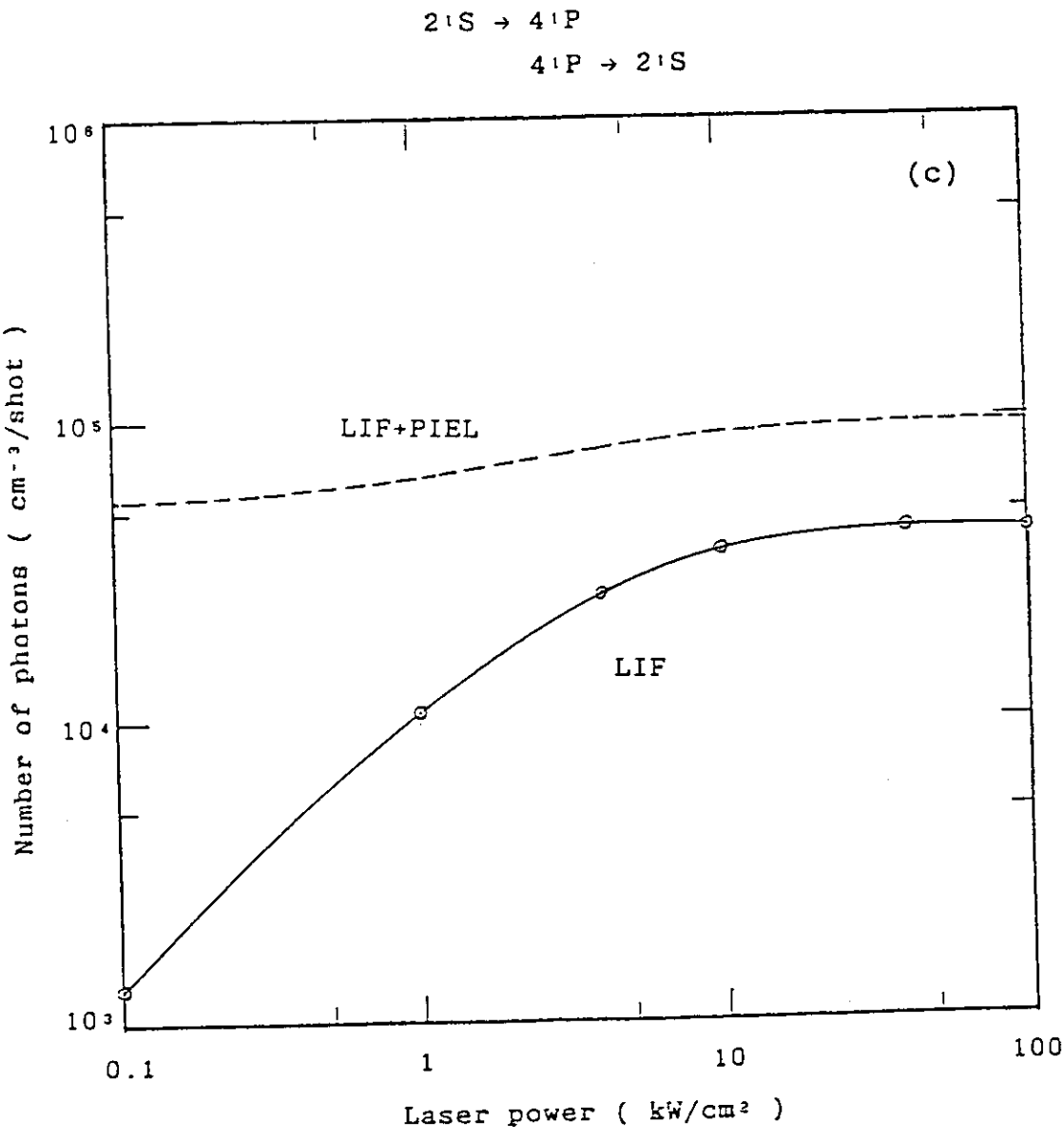

Fig. 10 (Continued)

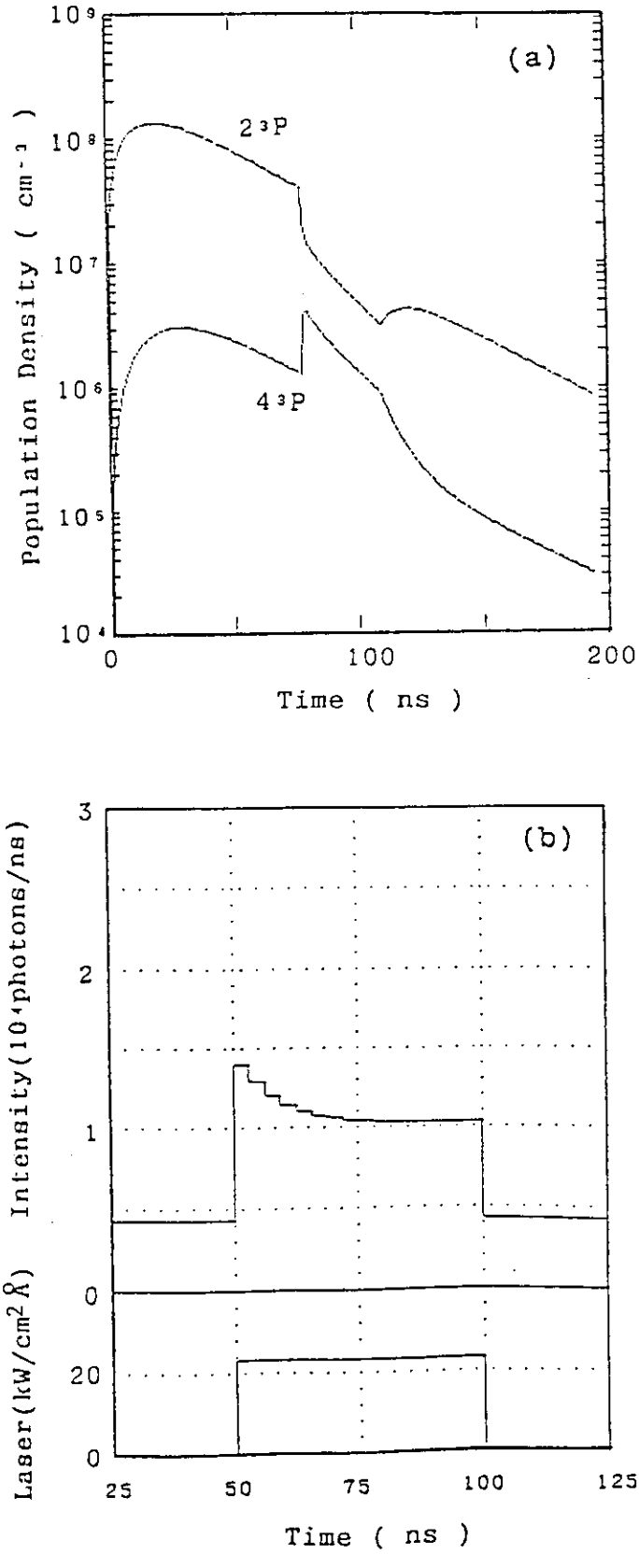

Fig. 11 Same as Fig. 9 except now for Case (3) of Table 2 and Fig. 4.

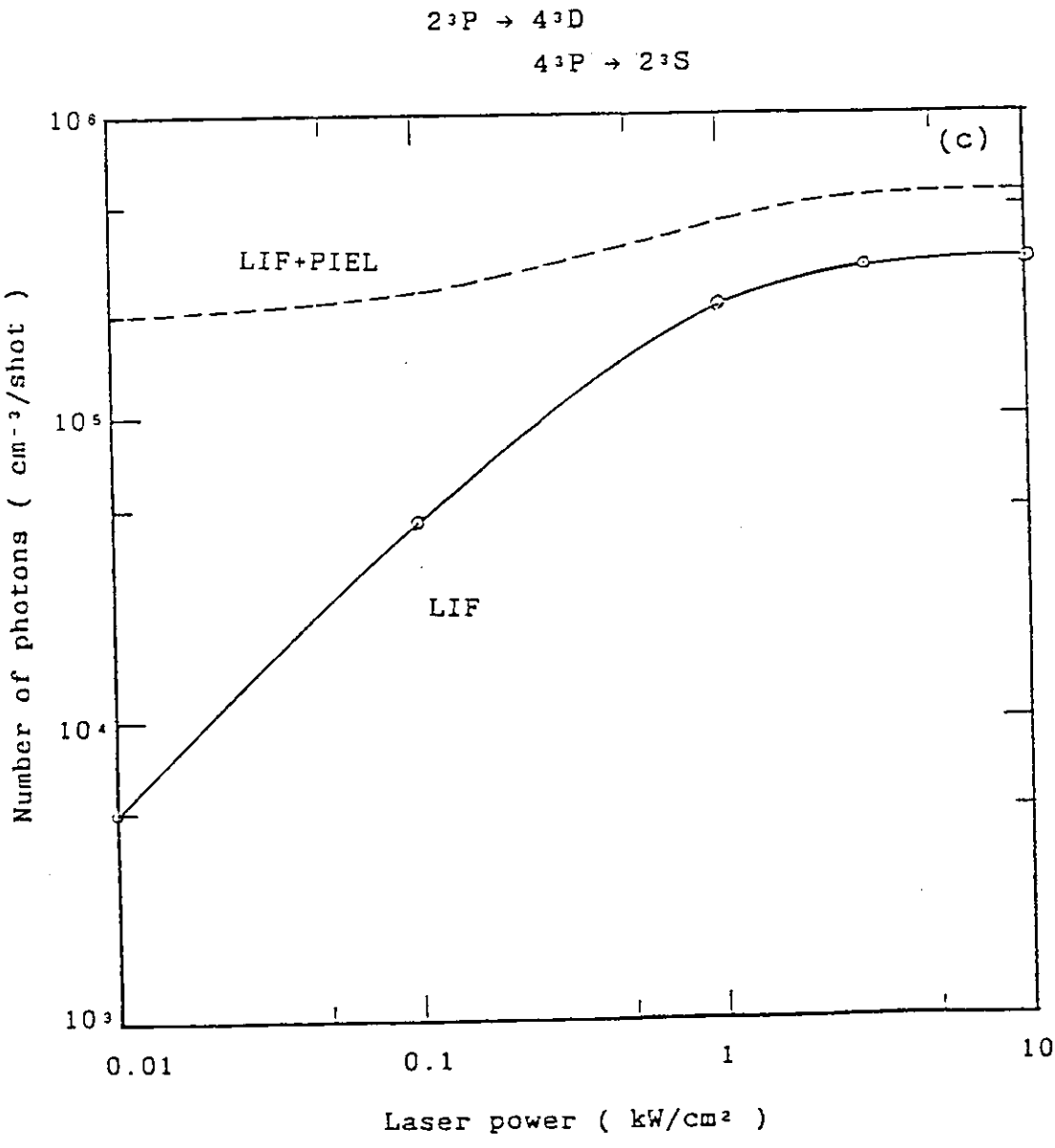

Fig. 11 (Continued)

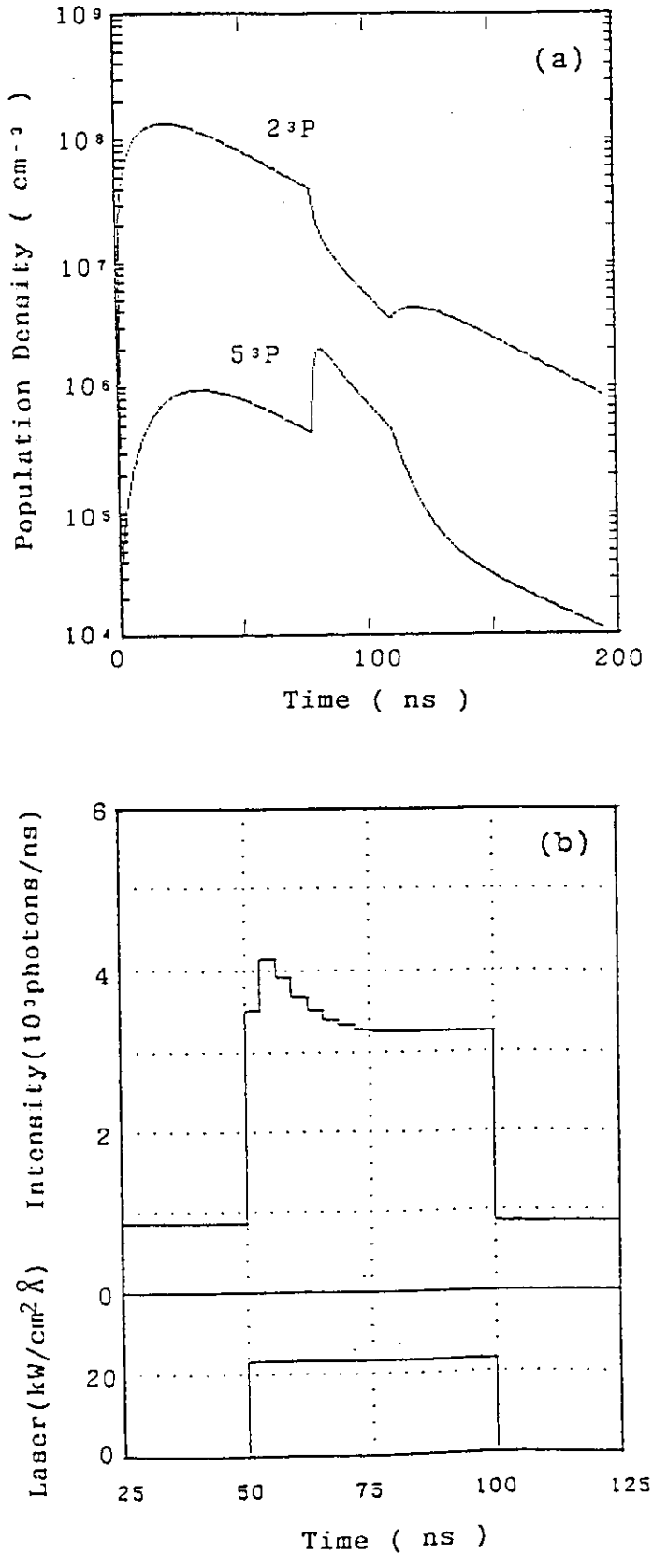

Fig. 12 Same as Fig. 9 except now for Case (4) of Table 2 and Fig. 4.

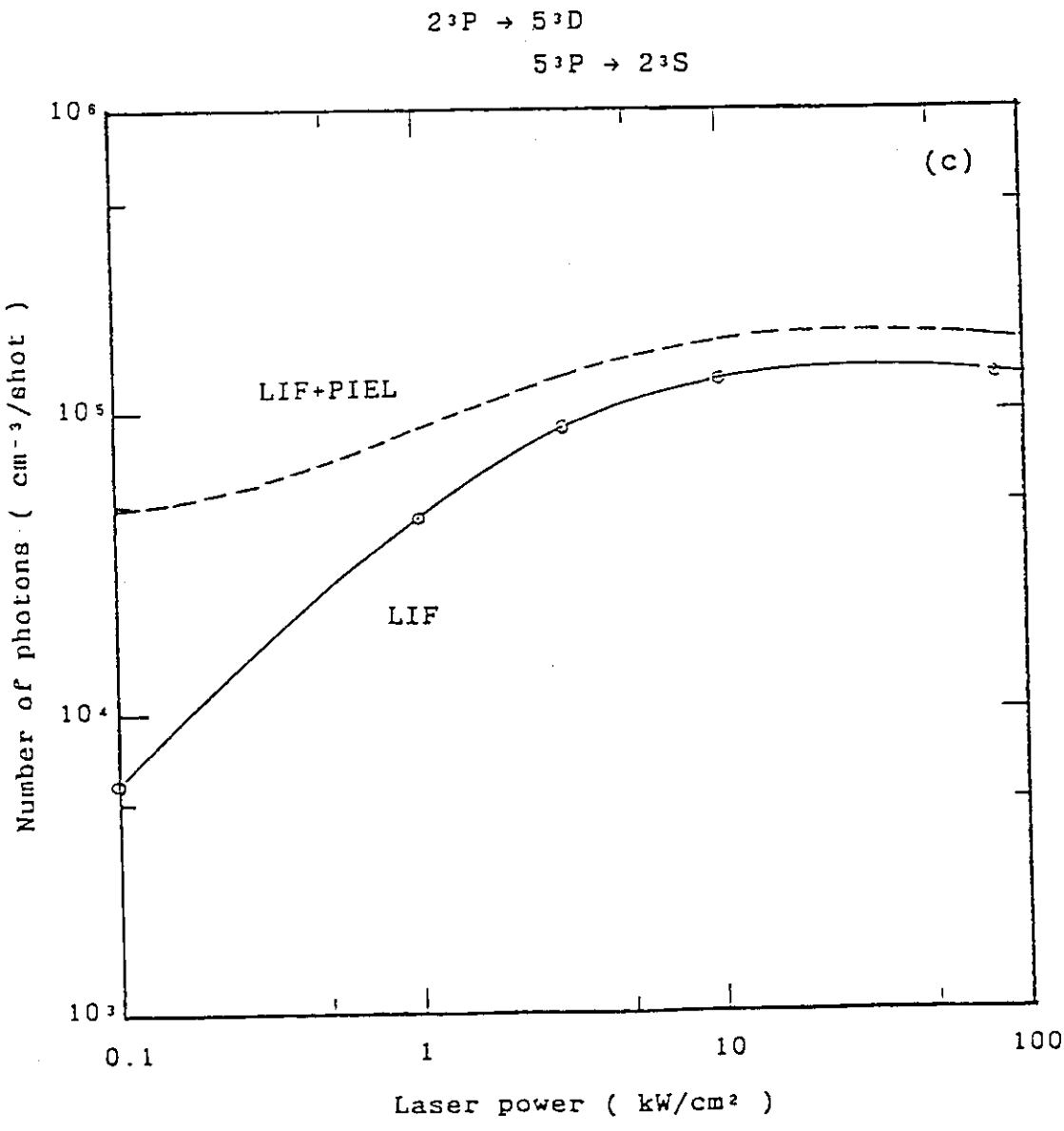

Fig. 12 (Continued)

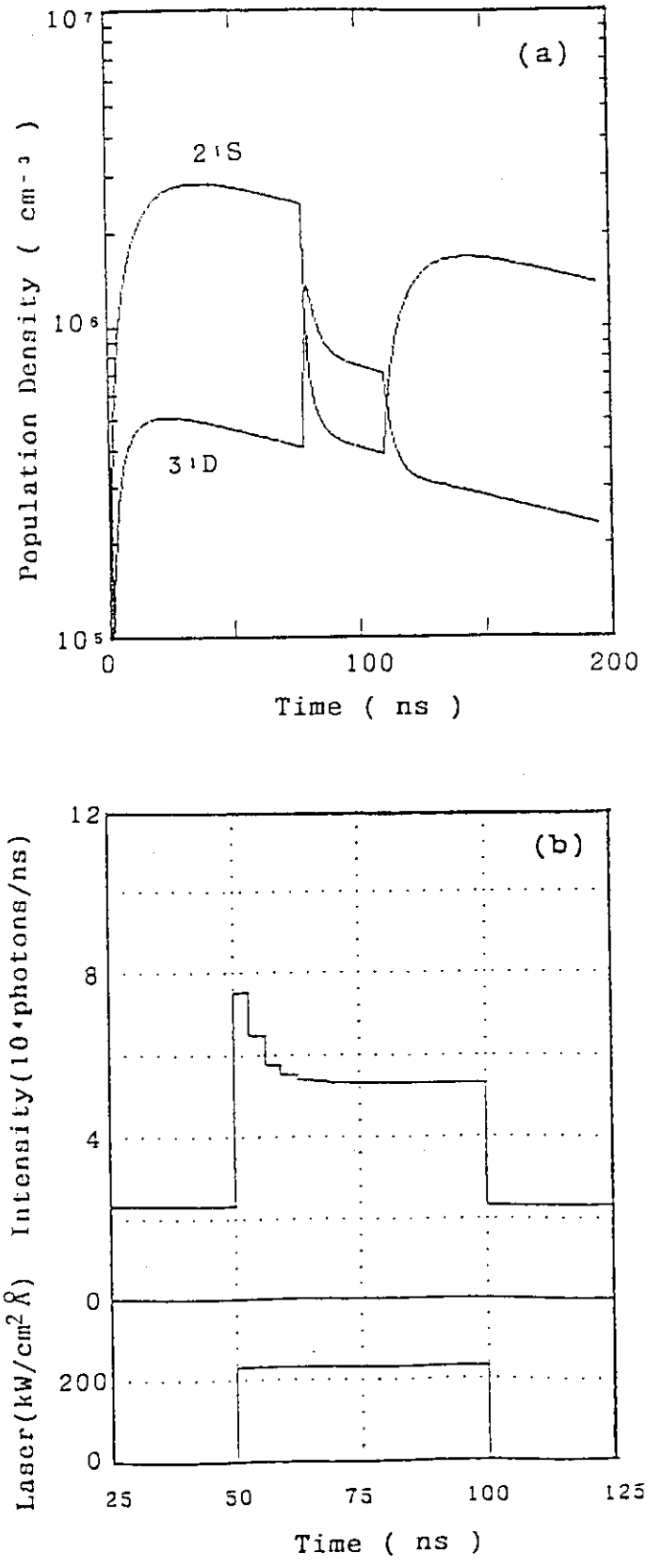

Fig. 13 Same as Fig. 9 except now for Case (5) of Table 3 and Fig. 4, which is a forbidden-excitation case.

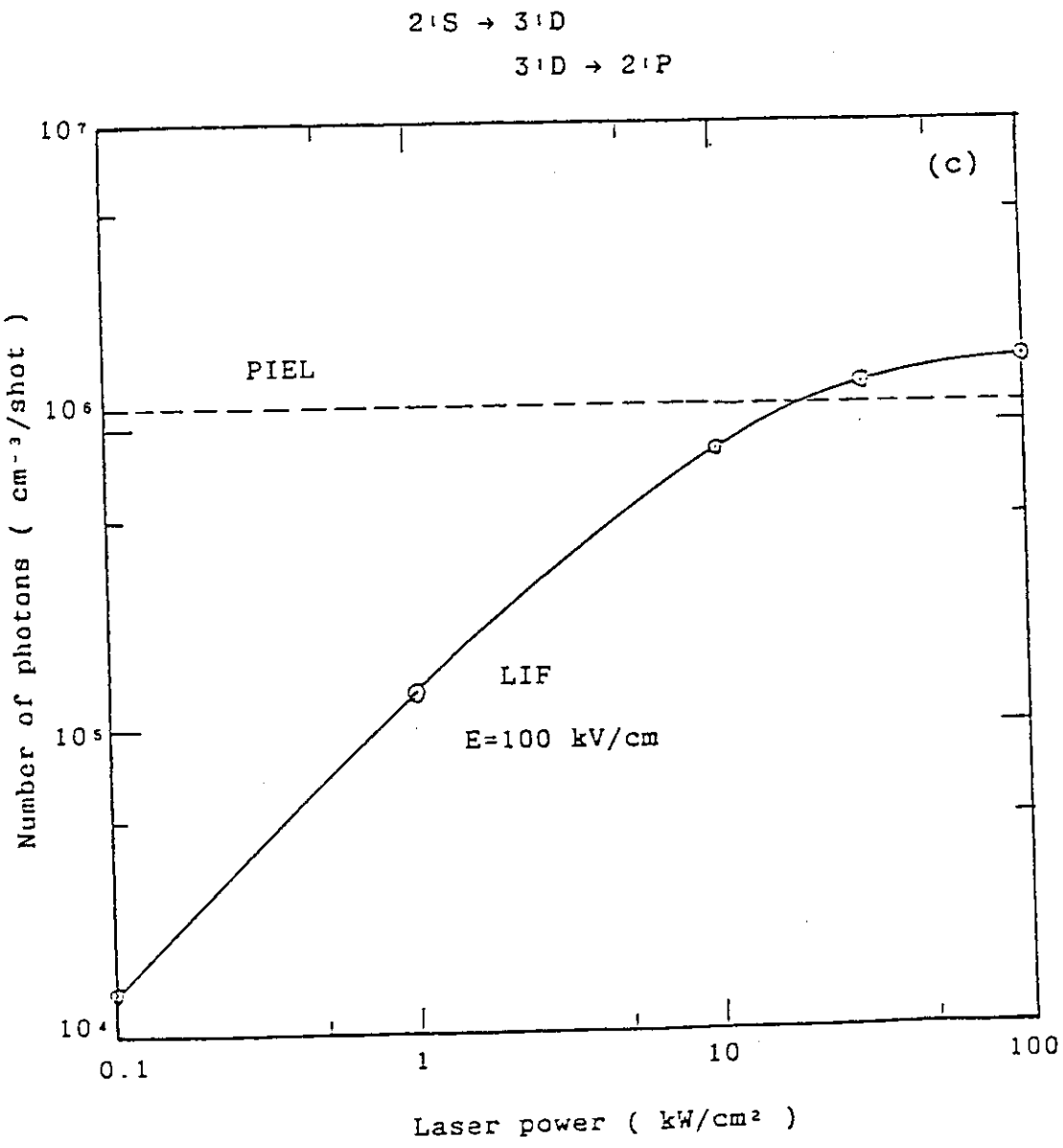

Fig. 13 (Continued)

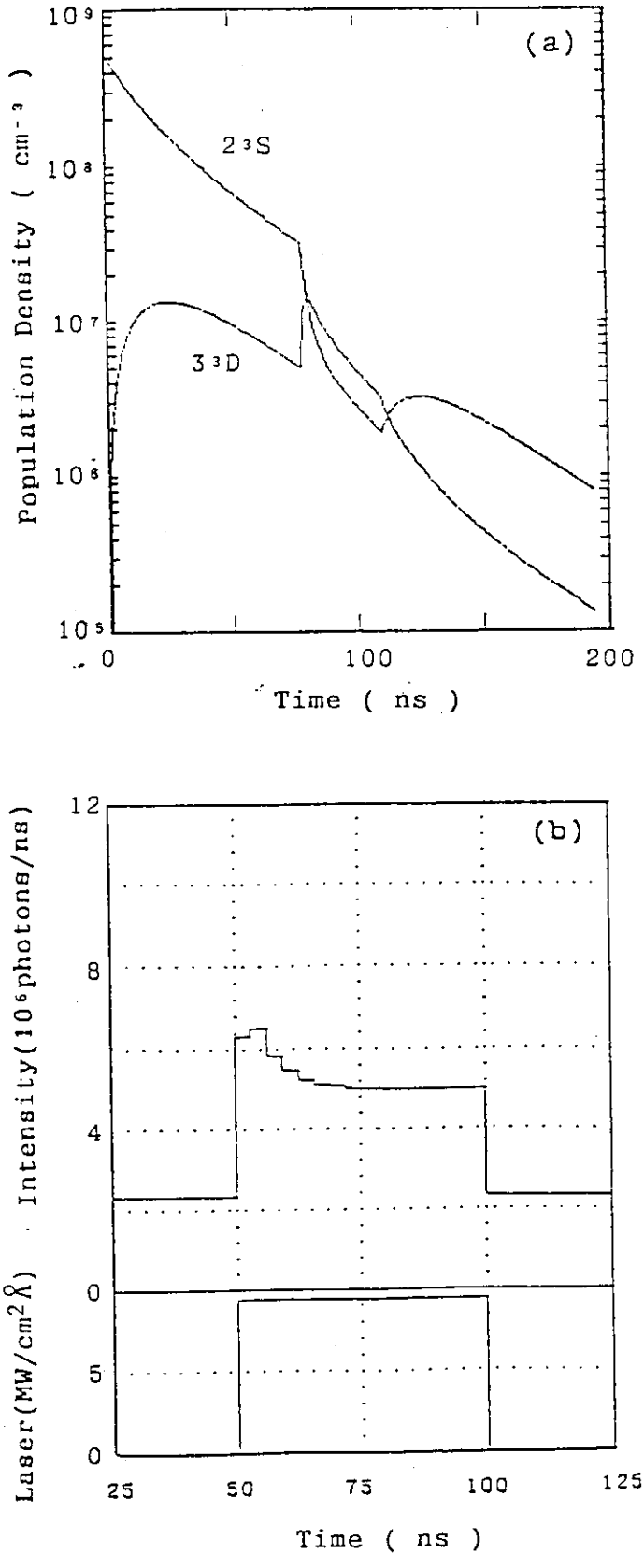

Fig. 14 Same as Fig. 9 except now for Case (6) of Table 3 and Fig. 4, which is a forbidden-excitation case.

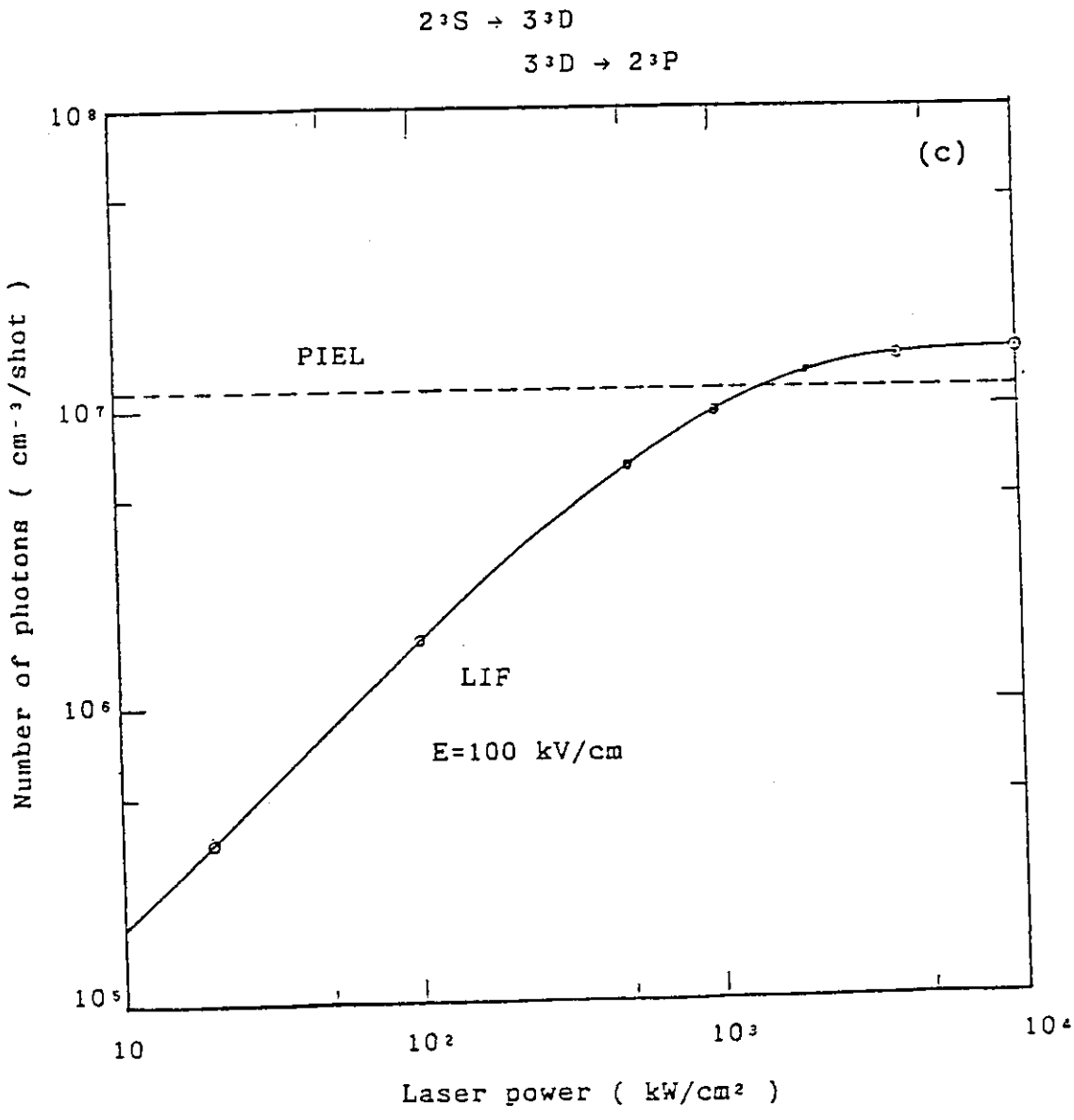

Fig. 14 (Continued)

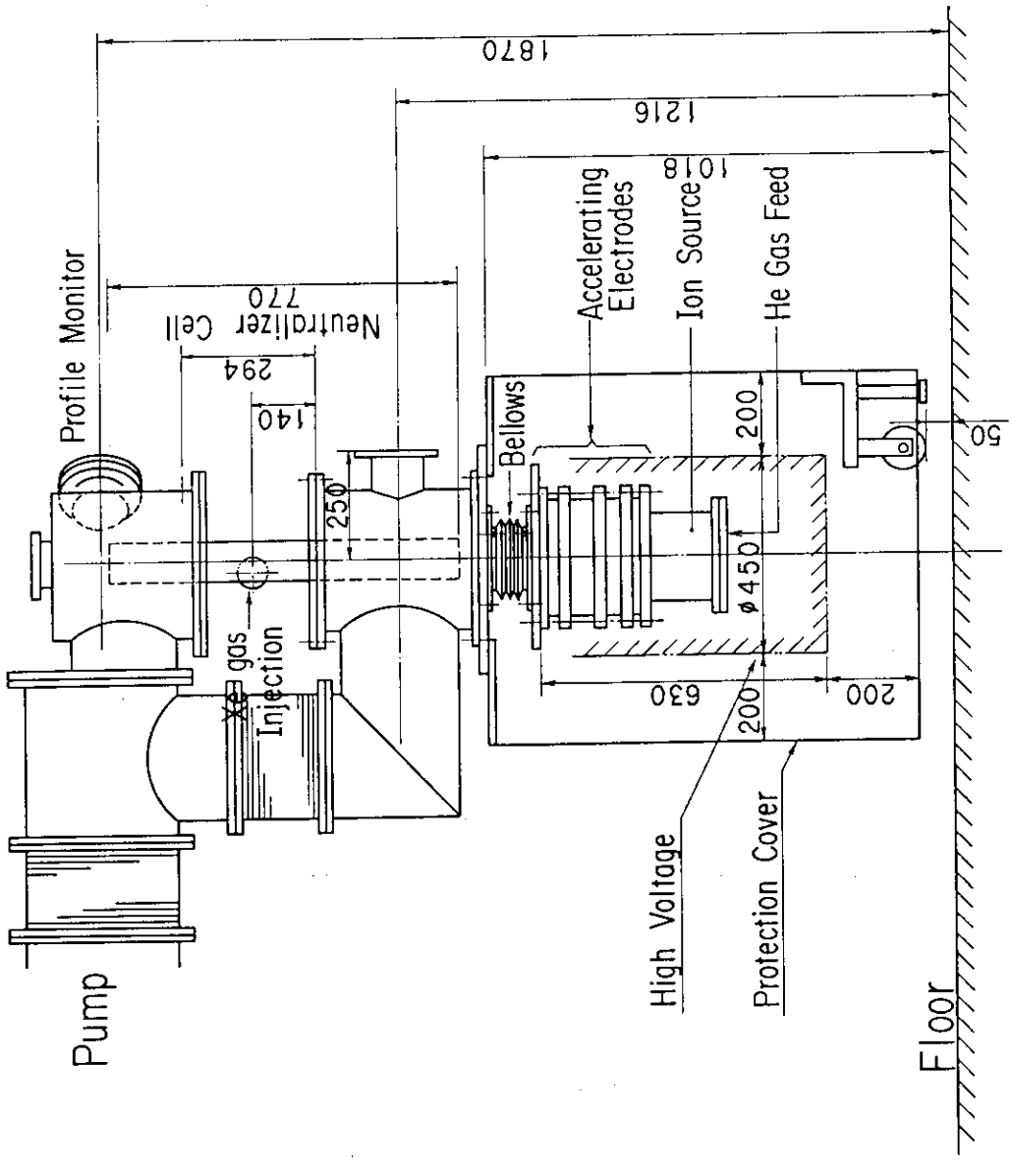

Fig. 15 Neutral helium-beam system for LAPPS, including dimensions.

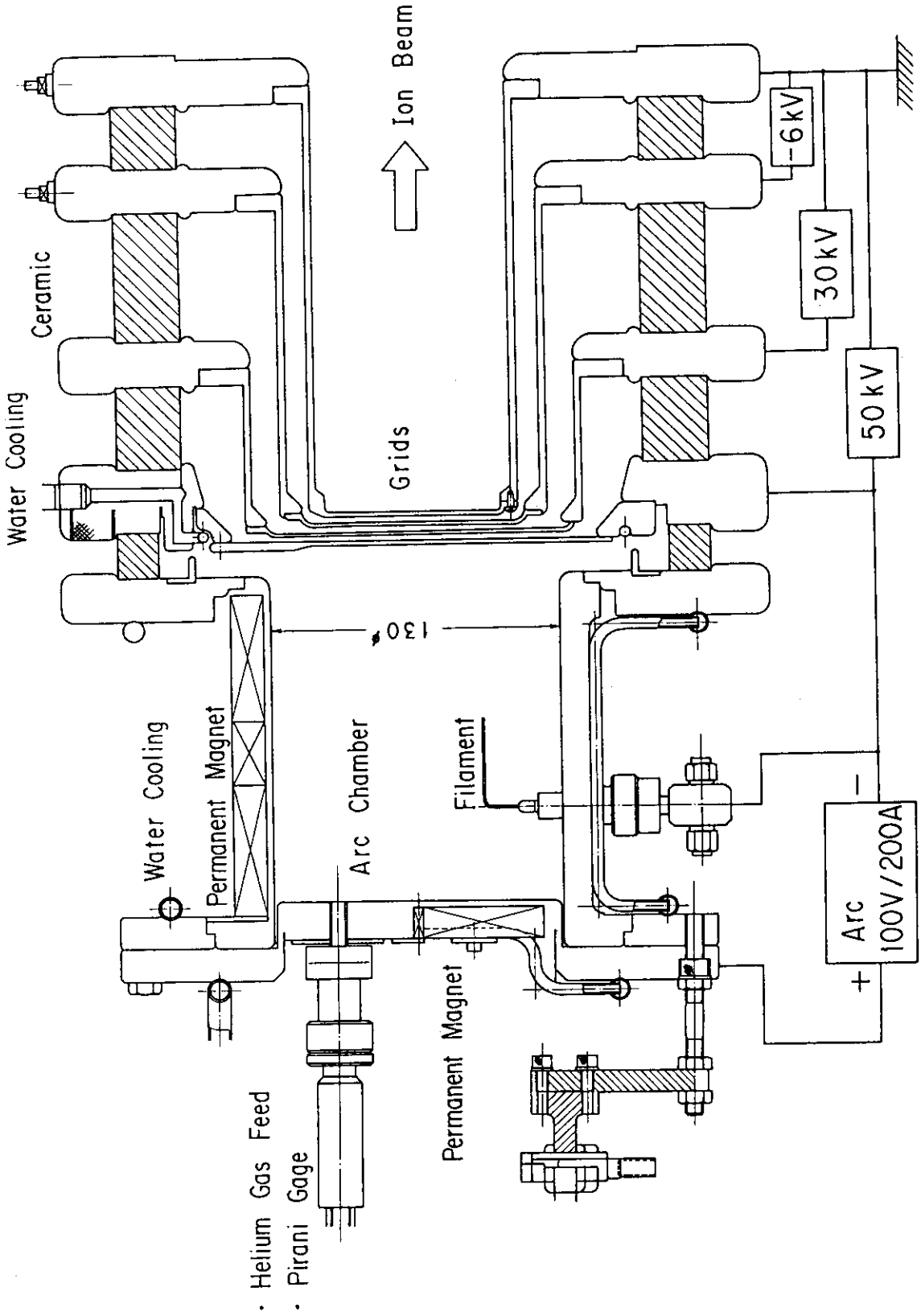

Fig. 16 Drawing of the helium-beam ion source.

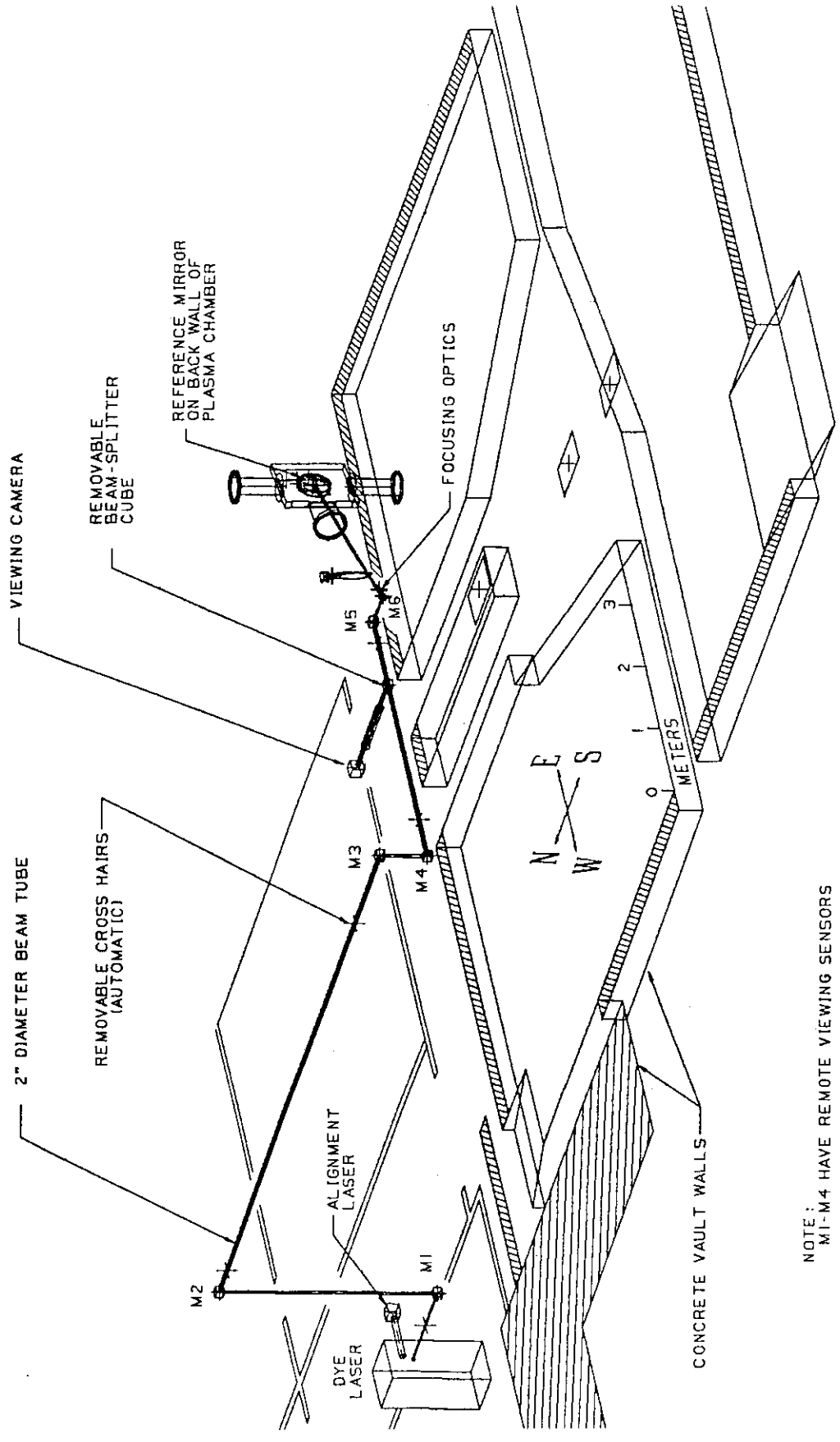

Fig. 17 Three-dimensional drawing showing the dye laser and the optical system that transports the laser beam to the tokamak plasma chamber. Components for the laser-beam alignment are also depicted. Beam-line turning mirrors are labeled M1 through M6.

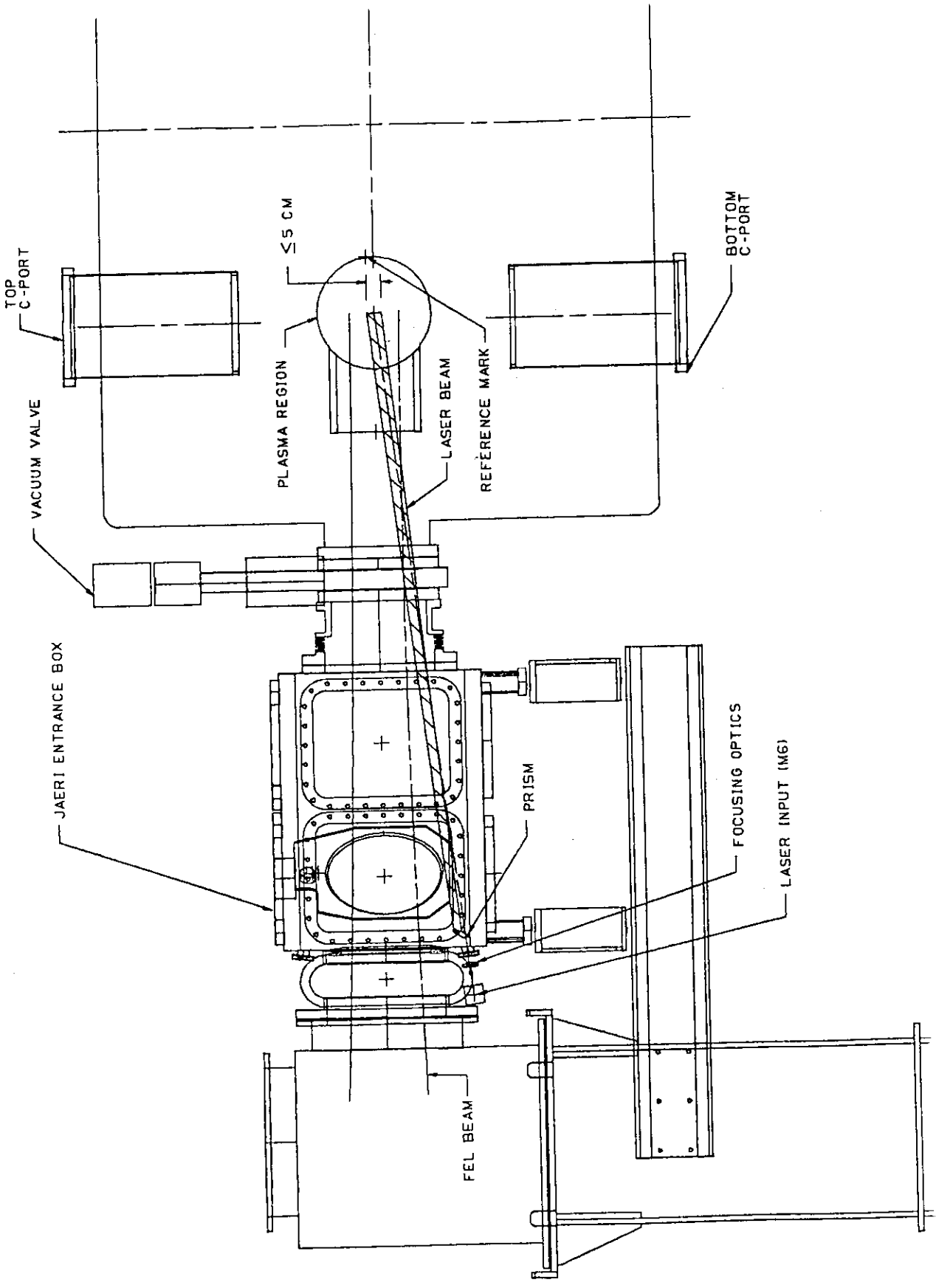

Fig. 18 Path of the laser beam from its entrance at the JAERI box to the plasma.

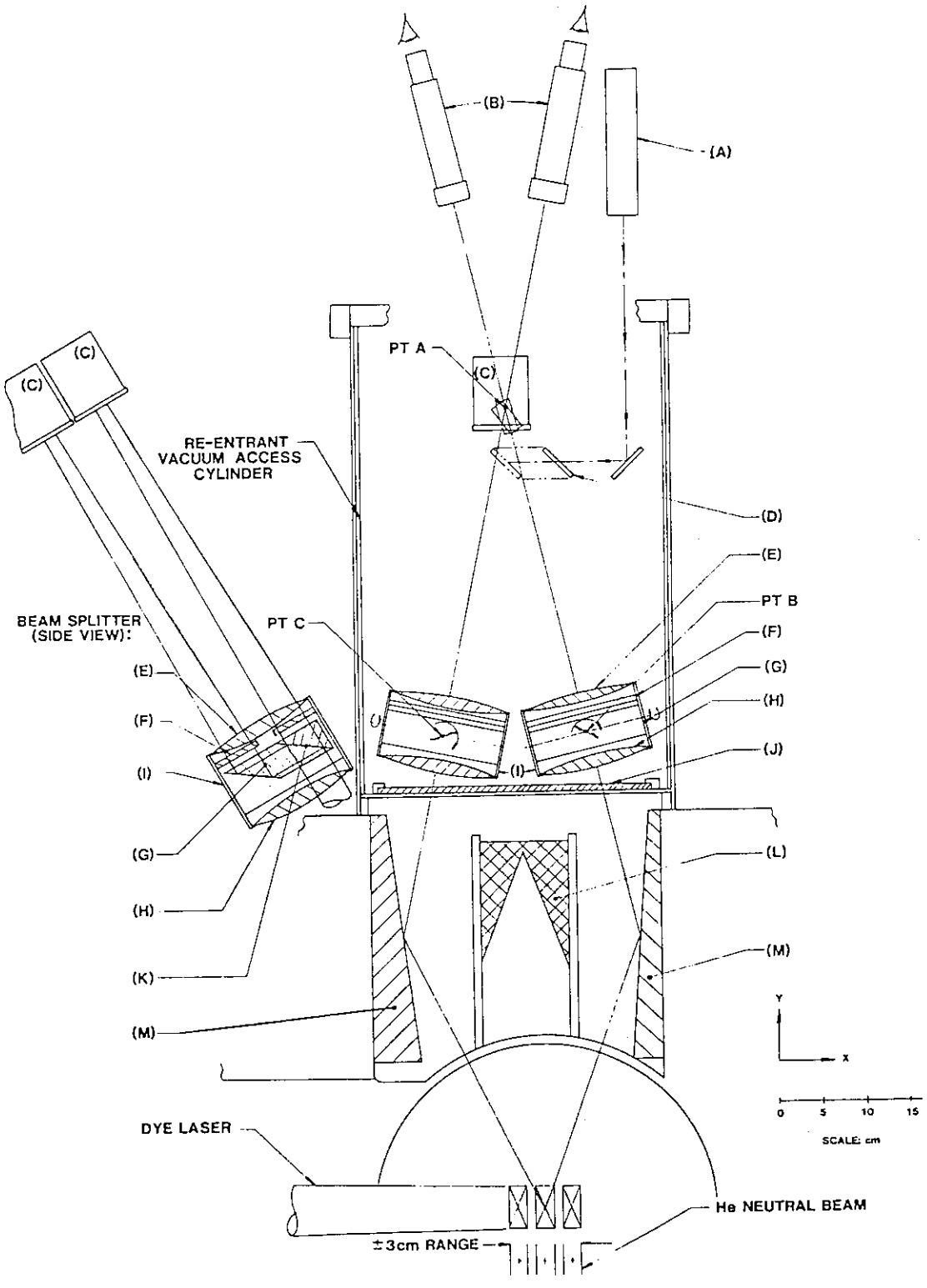

Fig. 19 Possible configuration for the LAPPS light-collecting optics. Parts shown include: (A) detector calibration source, (B) alignment-telescope positions, (C) detectors (translatable in the X direction), (D) insertable mirrors, (E) focusing lens, (F) wavelength filters, (G) prism, (H) collimating lens, (I) beam-splitter housing, (J) vacuum window, (K) dichroic surface, (L) helium-beam dump, and (M) fixed mirror mount. Cross hairs will be positioned at points A, B, and C during alignment. Outside the vacuum access cylinder at the left is a side view of the beam-splitter system inside the cylinder.

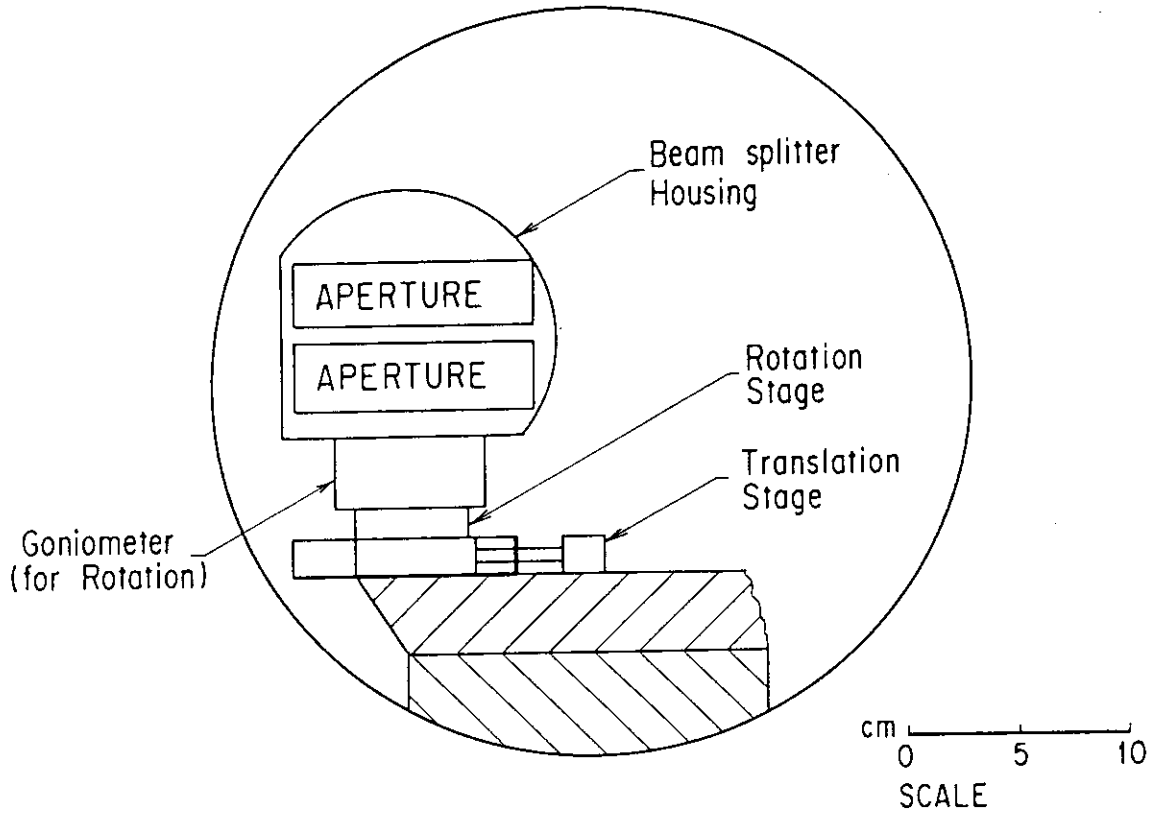

Fig. 20 This end view shows the three adjustment stages for the beam-splitter assembly of the light-collecting optics. (Side views are shown in Fig. 19.)

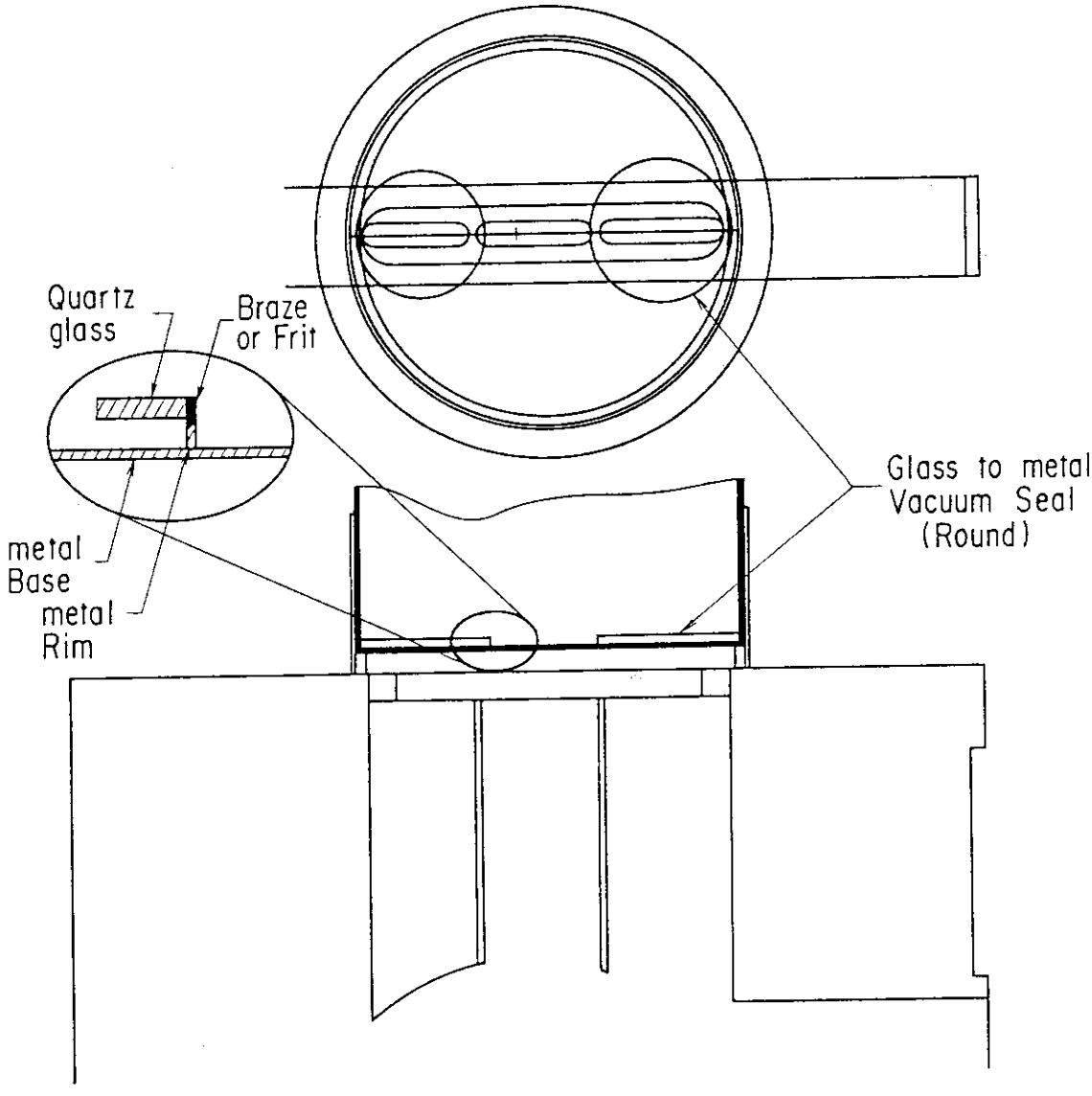

Fig. 21 A possible quartz-to-metal configuration for the vacuum seal of the windows of the LAPPS detection system.

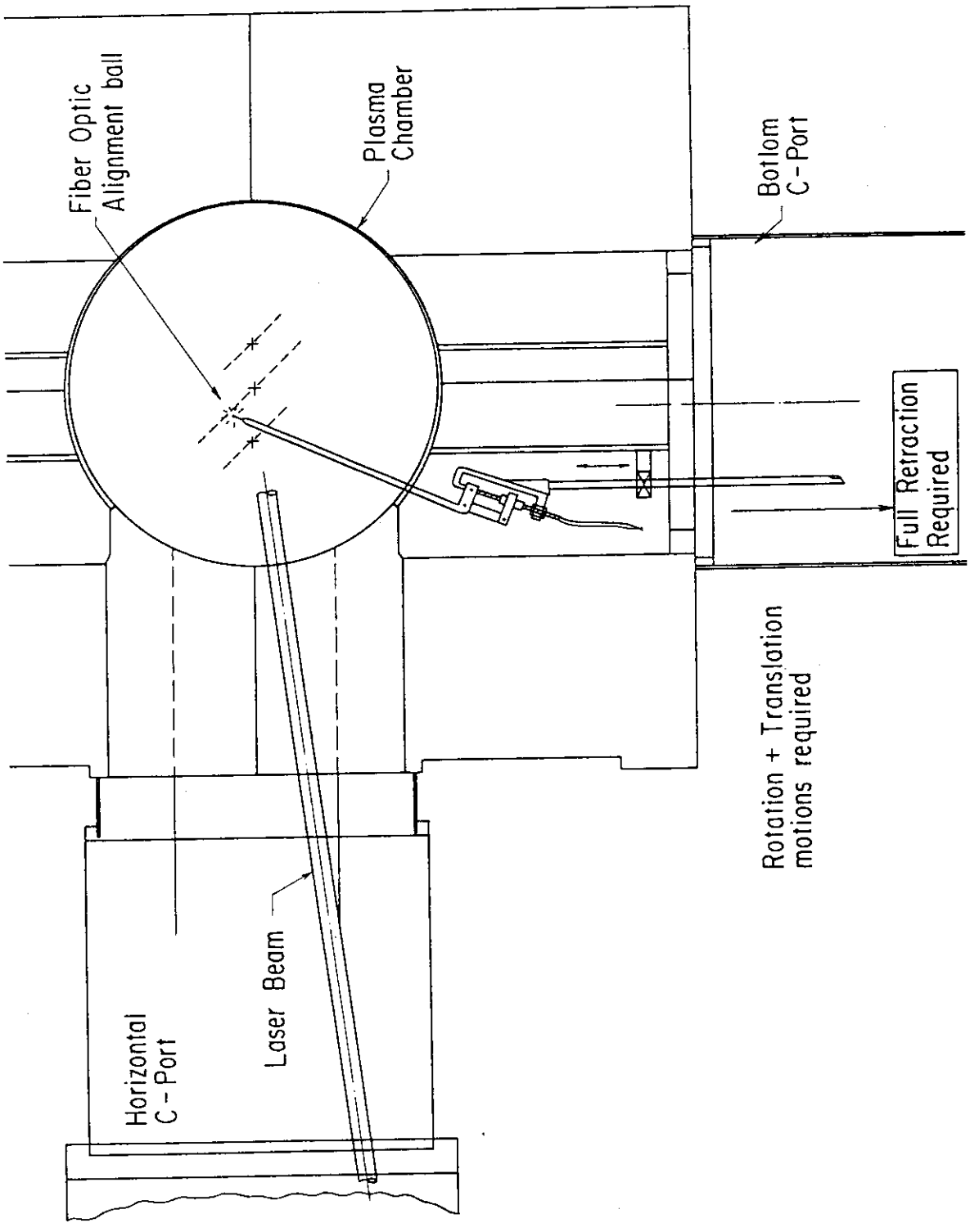

Fig. 22 Possible scheme for the inserting, adjusting, and retracting mechanism of the fiber-optic alignment ball.

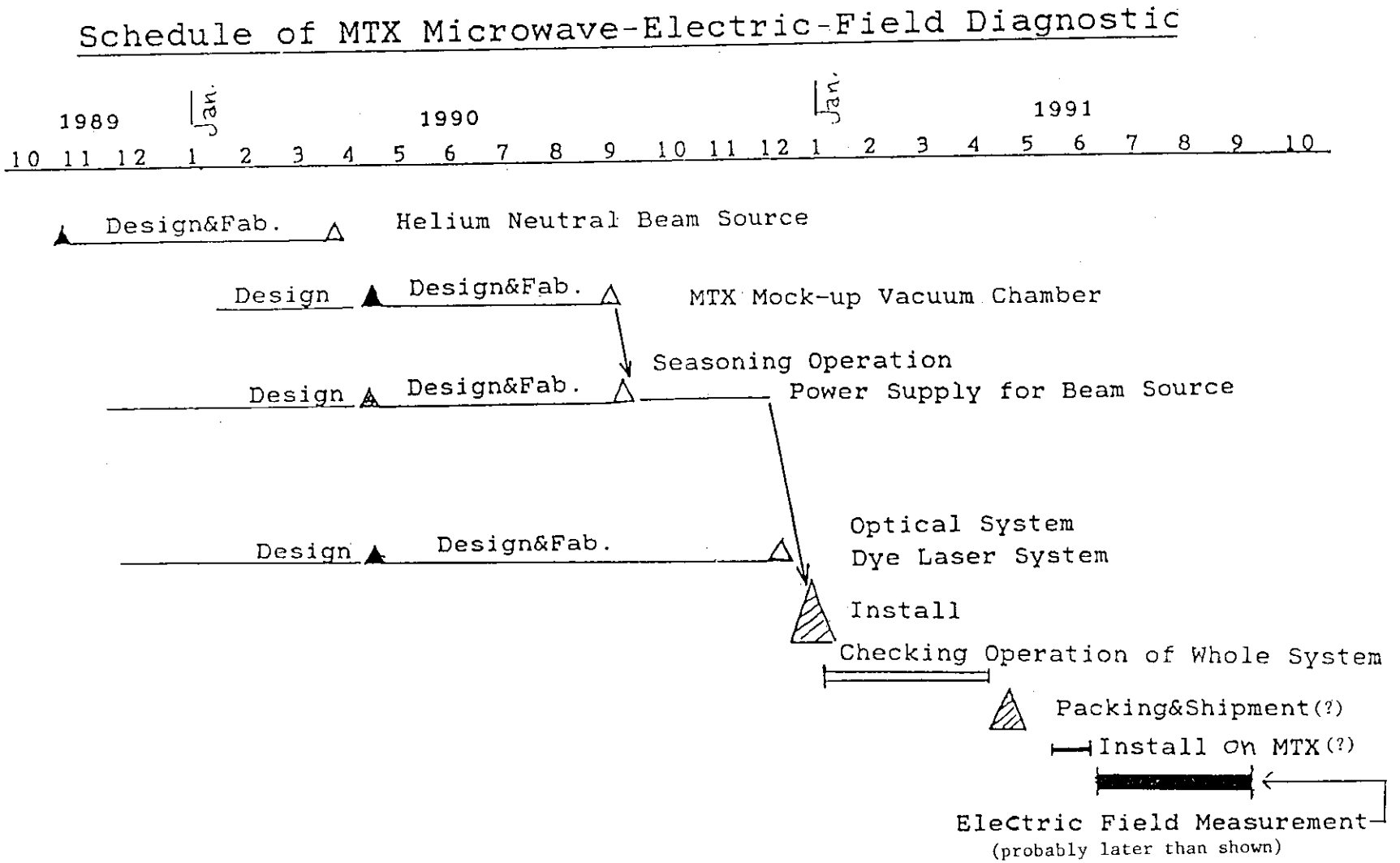

Fig. 23 Present schedule for progress on LAPPS.

Appendix 1 Abstract submitted for the Eighth Topical Conference on High-Temperature Plasma Diagnostics.

Stark-Effect Measurement of High FEL Electric Fields in MTX by Laser-Aided Particle-Probe Spectroscopy.* T. ODA,& K. ODAJIMA,# K. MIZUNO,@ K. OHASA,# M. SHIHO,# K. TAKIYAMA,& J.H. FOOTE,+ and D.G. NILSON+ -- We are constructing a diagnostic system to measure the electric field (>100 kV/cm) of a free-electron laser (FEL) beam when injected into the plasma of the Microwave Tokamak Experiment (MTX). The apparatus allows a crossed-beam measurement, with 2-cm spatial resolution in the plasma, involving the FEL beam (with 140-GHz, ≈1-GW ECH pulses), a neutral-helium beam, and a dye-laser beam. After the laser beam pumps metastable helium atoms to higher excited states, their decay light is detected by a collimated optical system. Because of the Stark effect due to the FEL electric field ($\vec{E}$), a forbidden transition can be strongly excited. The intensity of emitted light resulting from the forbidden transition is proportional to E^2. Because photon counting rates are calculated to be low, extra effort is made to minimize background and noise levels. It is possible that the lower $\vec{E}$ of an MTX gyrotron-produced ECH beam with its longer-duration pulses also can be measured using this method. Other applications may include measurements of ion temperature (using CXR), edge-density fluctuations, and core impurity concentrations.

* Performed by Lawrence Livermore National Laboratory+ for USDOE under Contr. W-7405-ENG-48 and by Japan Atomic Energy Research Institute,# Ibaraki, Japan.

& Hiroshima University.

@ Plasma Physics Research Institute and U.C., Davis.

Appendix 2 Calculation of the total photon number N_p for PIEL and LIF emitted per unit volume in the observing time Δt (see Sec. 3).

1. PIEL Component.

The photon-emission rate from the neutral-helium beam due to PIEL in the observation region from x_1 to x_2 in Fig. 8(a) is defined by

$$r_{PIEL} = A_{ki} \cdot \int_{x_1}^{x_2} n_k(x) \cdot S \, dx \ ,$$

where S is the cross section of the beam. Then, the total number of photons emitted from the beam within the observation region, whose volume is $(x_2 - x_1) \cdot S$, can be written as

$$N_{PIEL} = r_{PIEL} \cdot \Delta t \ ,$$

where Δt is the observing time.

2. LIF Component.

When the beam is excited by a pulsed laser, the population density should be treated as a function of x and t, i.e., $n_k(x,t)$. Let the laser illuminate uniformly the observation region $(x_2 - x_1)$ in the beam during $t = 0$ to Δt.

First, we examine the volume element $\Delta V = S \cdot \Delta x$ in the beam traveling with speed v_b. When the element arrives at $x = x_1$ (at $t = 0$), the atoms in the element can be excited by the laser only for a transit time $T_{tr} = (x_2 - x_1)/v_b$ from position x_1 to position x_2 (we assume $T_{tr} < \Delta t$ in the present case). Then, an enhancement in the density of the excited state k is induced, for example, as shown by the hatched region in Fig. 9(a) for level 3^1P. We express this quantity at $x = x_1$ by $\Delta n_k(x_1,t)$; this reference quantity will be used below.

Next, we present the time dependence of the density enhancement for each volume element, these elements being at various locations when the laser is fired (at $t = 0$):

[a] For elements within the region A ($x_1 < x < x_2$) at $t = 0$, the enhancement is given by

$$\Delta n_k^A(x,t) = \frac{n(x)}{n(x_1)} \cdot \Delta n_k(x_1,t) \ ,$$

where $0 < t < (x_2-x)/v_b$.

[b] For elements within the region B $(x_1-v_b\Delta t < x < x_1)$ at $t = 0$, the enhancement is given by

$$\Delta n_k^B(x,t) = \Delta n_k(x_1, t-(x_1-x)/v_b) \ ,$$

where $(x_1-x)/v_b < t < \Delta t$.

Thus, the photon-emission rate for LIF can be written as

$$r_{LIF}(t) = A_{ki} \cdot S \cdot \left[\int_{x_1}^{x_2} \Delta n_k^A(x,t)\ dx + \int_0^{x_1} \Delta n_k^B(x,t)\ dx \right] .$$

Finally, the total photon number by LIF is obtained from

$$N_{LIF} = \int_0^{\Delta t} r_{LIF}(t)\ dt \ .$$